NATIONAL UNIVERSITY OF SCIENCE AND TECHNOLOGY POLITEHNICA BUCHAREST

DOCTORAL SCHOOL OF ELECTRICAL ENGINEERING

SUMMARY

Finite element analysis and diagnosis of electrical machines faulty operation states

PhD Thesis

Scientific coordinator:

Prof. Phd. Eng. Virgiliu FIREȚEANU

PHD Student:

Eng. Alexandru-Ionel CONSTANTIN

BUCHAREST

2023

CONTENT

CHAPTER 1 STATE OF THE ART IN DIAGNOSTIC OF FAULTS IN ELECTRICAL MACHINES

1.1. Introduction

Fault detection and safety mechanisms are as old as electrical machines themselves. Customers and manufacturers used to rely on simple protection schemes like overcurrent, overvoltage, earth-fault, and so on to ensure safe and dependable performance.

However, as the complexity of the jobs performed by these machines increased, so did the need for improved defect detection methods. Unexpected machine downtime can disrupt workflow and cause significant financial losses. As a result, early fault identification has become critical.[1]

According to research on the durability of electrical machines, any component can fail, and the possibility varies depending on the machine's type and design, operating conditions, and application [2,3]. For a long time, thermal/vibration supervision and off-line diagnostics were the primary mechanisms for monitoring the condition of electric devices.

In this thesis, A study of faults three type of faults and their combinations using 3D finite element models for an induction machine, and some experimental results are presented. The discussed and proposed diagnostic technique can be extended and applied also to other kind of machines. In this chapter are presented information related to sources of faults for induction motors, types of faults, mechanisms of fault and faults diagnosis methods.

1.2. Sources of faults in the induction motors

In order to understand the occurrence of the fault and in order to build a scheme for the fault's detection, the sources and causes of induction motors damage must be known.

Table 1.1 presents the main sources of damage and types of faults with consideration to electrical motors, as Al-Kazzaz proposes in [4].

Table 1.1 Damage sources and types of faults with respect to electrical motors

SOURCES OF FAULTS				
INTERNAL SOURCE		EXTERNAL SOURCES		
MECHANICAL	ELECTIRCAL	MECHANICAL	ELECTIRCAL	ENVIRONMENTAL
- coils shifting - strikes of the rotor, bearings faults - eccentricity	- insulation faults - interrupted rotor bars - faults of the magnetic circuit	- pulsating charge - overcharge - faulty mounting	- transient voltages - unbalanced voltages - voltage variations (no charge, interruptions, low variations	- temperature - humidity - dust - fungi

This classification is useful in analysing the causes of faults and for determination of the maintenance plan which requires knowledge of the level of electrical, mechanical and environmental stress that may produce faults.

Taking into account the probability of occurrence, the faults in the electrical motor can be divided in four principal groups [5]: the most important share is that of bearing faults (40%), followed by the stator faults (38%) and by rotor faults (10%).

1.3. Types of faults in the induction motors

The overall distribution of faults in electrical machine (EM) varies depending on the specific machine type and its operational parameters. As illustrated in [6], conventional faults in electrical machines can be classified as electrical, mechanical, thermal environmental, and control faults. These faults are defined in [7–9].

Electrical faults are the most common type of fault in electrical machines, occurring primarily on the stator. They can occur as a result of insulation failure, short circuits, open circuits, or other issues with the machine's electrical components. The following are some of the most common causes of electrical faults: Defects in the stator that cause a phase winding to open or short; Improper connection of stator windings; Phase reversal; Over or under voltage; Inter-turn short circuit fault; Earth fault; Common-mode current (CMV) and bearing-current (BC).

Mechanical faults are the second most common type of fault in electrical machines, following electrical faults. These can be caused by worn bearings, misaligned shafts, unbalanced loads, or other mechanical issues with the machine. This type of fault is most commonly found on an electrical machine's rotor. Mechanical faults are classified into the following categories: Eccentricity fault; Damaged rotor end rings or shattered bars on the rotor; Broken bearings, damaged gearbox, and shorted rotor winding; A bending shaft may cause a fraction between the stator and the rotor, damaging the winding; Broken rotor bar (labelled as BB).

Thermal faults: The most common causes of these problems in electrical machines are bearing damage and insulation failure, both of which raise the temperature of the machine. The following are the primary causes of thermal faults: Overheating; Insulation breakdown; Overloading.

Environmental faults: When compared to the above-mentioned faults and their occurrence, environmental faults are the least common in electrical machines. The most common causes of environmental faults are machine exposure to water, dust, and humidity, which causes rusting and other types of damage. This can happen on both the stator and the rotor. Some examples of environmental faults are: Ambient temperature; Moisture; Vibrations.

Control faults: These can occur as a result of problems with the control system or software, causing the machine to operate incorrectly or fail. Electrical machine control faults are classified as: Software malfunction; Sensor failure; Power supply failure.

Electrical faults are the most common type of issue in electrical machines. The next most common type of issue is mechanical failure. However, the specific distribution of faults can differ depending on the type of machine and its operating conditions, as shown explicitly in Table 1.2.

Table 1.2 Numerous electrical machine faults and the most recent fault diagnostic trends

Fault Category	Description	Classification	Reference
Electrical	Phase winding opening/short	Stator	[10]
	Improper winding connection	Stator	[11,12]
	Phase Reversal	Supply	[13]
	Over or under voltage	Supply	[14-17]
	Inter turn short circuit	Winding	[12,18]
	Broken rotor bar/end ring	Rotor	[19-25]
	Stator open/short circuit	Stator	[26]
	Insulation damage	Stator	[27-29]
Mechanical	Eccentricity	Rotor	[27-29]
	Mechanical unbalance	Rotor	[25,30,31]
	Bearings failure	Rotor	[32,33]
	Bending shaft	Rotor	[34-36]
			[37]
Thermal	Over heating	Winding	[38,39]
	Insulation breakdown	Winding	[40]

Fault Category	Description	Classification	Reference
	Over loading	Winding	[41-43]
	Thermal unbalance	Rotor	[44-46]
Environmental	Ambient temperature	Enclouse	[47-49]
	Moisture	Environmental	[48,49]
	Vibrations	Rotor	[38]
Control	Power supply failure	Supply	[50]
	Current sensor fault	Sensor	[51]
	Voltage sensor fault	Sens	[52]
	Speed sensor fault	Sens	[52-56]

Due to the coupling effect between various state variables of electrical machines, one kind of fault can give rise to the other faults. For example, if some bars are broken, the net flux linkage is no longer zero, giving rise to the eddy current in the shaft and bearings.

1.4. Types of Condition Monitoring and Faults Diagnostic techniques

This section thoroughly examines the techniques for adapted condition monitoring and fault diagnosis, highlighting the most efficient and useful methods. For determining the health of an EM drive system, both invasive and non-invasive methods can be used for fault diagnosis. This method of defect detection does not require direct contact with the motor drive system under investigation [57]. Using measurements or signals from outside the system, these techniques analyse the system's behaviour and look for potential problems. Invasive fault diagnostic methods entail making direct contact with the system in order to pinpoint its flaws.

Common condition monitoring (CM) methods that use sensory data and electrical signature analysis (ESA) are useful for evaluating the state of EM, particularly induction machine (IM). Motor current signature analysis (MCSA) is widely accepted as the industry standard method for analysing signatures in IM fault detection. The current signal signature is examined and interpreted in order to identify and locate potential problems within the motor system [58]. ESA includes motor circuit analysis in its evaluation process. Resistance, phase angle, current response (CR), frequency response (FR), and comparable impedance, inductance, and ground faults are all part of the process. Several condition monitoring strategies have been used in the past to detect defects in electrical machinery. Several of these techniques are described here [59-67]: Analysis of the motor's current signature [68]; Analysis of voltage signatures [69]; The Extended Park approach [70]; The analysis of instantaneous power signatures [71]; The analysis of state surveillance parameters such as temperature, disturbances, speed variation, and magnetic flux; Condition monitoring sensors(Vibration sensors, such as accelerometers and proximity probes, are commonly utilized in various applications; Temperature-sensing equipment, including thermocouples and resistance temperature detectors; Current detectors, including hall effect sensors and current transformers; Microphones and ultrasonic sensors, which are included in the category of acoustic sensors; Monitoring based on emission levels.); Diagnostics involving surges and partial discharges; An examination of the motor circuit.

Multiple classifications exist for fault diagnosis procedures, such as invasive- and non-invasive-based methods, conventional techniques, signal processing, or model-based techniques. shows the different conventional techniques for fault condition monitoring.

The application of signal-based methodologies in the field of CM and the fault diagnosis of electrical machines entails the examination and analysis of multiple signals obtained from these machines. This analysis aims to identify any irregularities, deviations, or fault signatures that may

be present. [72]. The aforementioned methodologies primarily focus on the extraction of relevant data from the signals to evaluate the status of the machine... These signals encompass a range of parameters, such as vibration, current, temperature, and acoustic emissions, among others. By scrutinizing these signals, anomalies, deviations, or distinct fault signatures can be identified, providing critical insights into the operational health of the machines. By carefully interpreting signal patterns and variations, these techniques empower engineers and experts to pinpoint potential issues swiftly, enabling timely interventions and proactive maintenance strategies to mitigate downtime and optimize electrical machines' overall reliability and efficiency.

In signal-based techniques within condition monitoring and fault diagnostics, diverse signal processing methodologies are employed to extract fault features in the signature of sensor data. Together with fundamental approaches like the fast Fourier transform (FFT), short-time Fourier transforms (STFT), and time-frequency analysis (TFA). The Winger-Viile distribution, more sophisticated and advanced techniques such as the wavelet transform, the Hilbert-Huang transform, multiple signal classification (MUSIC), empirical mode decomposition (EMD), and cyclostationary analysis (CSA) are important. FFT and STFT are the most common signal-processing techniques for frequency spectrum analysis to trace the fault frequency in the signature of the sensor data. The wavelet transform offers a multi-resolution analysis, uncovering hidden features at various scales in both time and frequency domains. EMD dissects signals into intrinsic mode functions, facilitating the detection of complex and non-stationary fault patterns. CSA capitalizes on cyclic properties in signals, effectively identifying cyclostationary components linked to specific fault types. By harnessing this array of advanced signal processing techniques, condition monitoring and fault diagnostics achieve a comprehensive understanding of machine behaviour, enabling early detection and accurate diagnosis for optimized maintenance strategies.

The implementation of model-based methodologies for the CM and fault diagnosis (FD) of electrical machines relies on applying mathematical models to assess the performance of the motor and identify any pertinent problems or deviations from the established operational criteria [74,75]. Analytical models, finite element analysis (FEA), signal processing, Kalman filtering (KF) and state estimation, AI, stochastic resonance, and machine learning are the main model-based techniques used in FD. Model-based techniques offer significant benefits for electrical machinery CM and FD. These approaches enable the anticipation of defects, predictive maintenance (PJV1), enhanced dependability, and improved performance. The aforementioned categories can also be applied in the context of AI techniques utilized for diagnostic purposes. The implementation of PJV1 using AI requires the integration of human intelligence with machine learning techniques, namely the training of algorithms for the purpose of machine fault diagnosis. [76,77].

Academic and industrial sectors are currently investing significant resources into research and development (R&D) pertaining in CM and FD, specifically targeting problems arising from high-frequency inverter transients and their associated behaviours [78]. In this field, AI has significantly transformed the domain of the CM and FD of electrical machines. Techniques such as artificial neural networks (ANNs) employ intricately interconnected layers to learn intricate patterns from data, enabling accurate fault detection and classification,. Fuzzy logic and Adaptive fuzzy systems leverage linguistic variables to capture uncertainties in the system, facilitating robust decision making in complex scenarios of fault diagnostics. Also, support vector machines (SVM) excel at classification tasks by finding optimal decision boundaries within high-dimensional data. Expert systems combine domain knowledge with inference engines to mimic

human expertise, making them adept at diagnosing intricate faults. These Al-based methodologies have ushered in a new era of advanced condition monitoring, offering precision, efficiency, and adaptability for maintaining the health and longevity of electrical machines.

Advanced condition monitoring and fault diagnostic methods for induction motor faults have emerged due to advancements in technology and research. The authors present a list of more advanced and recent condition monitoring methods for induction machines faults, along with their types and further subtypes in Table 1.3.

Table 1.3. State-of-the-art techniques and the latest trends in condition monitoring and fault detection.

Latest Trends in Techniques	Feature Application
Advanced techniques in signal processing	• Time–domain analysis [80]: o Mean-square and amplitude analysis [81,82]; o Kurtosis testing [83]; o An investigation of harmonic order tracking [84]; o The time synchronous average, often known as TSA [85–87]; o Analyses of statistical data [88]; ▪ Stochastic resonance [89]. o Decomposition of signal. • Frequency–domain analysis: o The fast Fourier transform, abbreviated as FFT; o The wavelet transform [87]; o Spectral analysis at higher levels. • Time–frequency analysis [90,91]: o Spectrogram; The Hilbert–Huang transformation in addition to its extension: ▪ Obtaining the frequency and intensity of the instantaneous signal. o The short-time Fourier transform (also known as STFT); o Transformation of Wigner packets [92]. o Wavelet–Ville transform [93]; • High-resolution analysis techniques [94,95]: o MUSIC [96].
Computer-based intelligent technique	• Artificial intelligence [97]: • Data-driven approach [98–100]; • Machine learning (ML) [79]; o High-dimensional feature reduction [101,102]. • Data mining: date fusion and pattern recognition [103].
Expert Systems	• Rule-based systems [104,105]; o Fuzzy logic [106]. • Case-based Reasoning [107]: o Experience-based reasoning.
Prognostics and health management (PHM)	• Recognition of more complex diagnoses by technological advancement [108]; • Smart classifier-based prognostics [109].

1.5. Thesis description

Chapter one presents some sources of faults for the induction motors, types of faults in induction motors, numerous electrical machine faults and the most recent fault diagnostic trends, types of condition monitoring and faults diagnostic techniques, traditional types of condition monitoring and some of the latest trends and developments in condition monitoring. The characteristics of the induction machine used as reference for the 3D finite element models developed using Altair Flux 3D software for the analysis of the fault's detection, evolution and influence on torque, unbalanced force, currents and magnetic field in the proximity of the machine are presented in **Chapter two**. The induction machine is produced by UMEB and was chosen because has 3 more additional external connections on one phase after first, second and the fourth elementary coils, used to simulate the short-circuit fault. Also, the finite models developed are described for each studied fault and the formulation of the electromagnetic field. **Chapter three** analyses the influence the individual faults and their combination on electromagnetic torque in rated load motor operation (2880 rpm) and **Chapter four** presents the influence of the faults on the rotor unbalanced force that's acts on the rotor. Results related to the detection of mono, double and triple faults in the squirrel-cage induction motor through theirs influence on the harmonics of the stator currents in load (2880 rpm) are presented in **Chapter five.** Regarding **Chapter six**, the most important one of the thesis, presents related to the influence of the individual faults and theirs combination on the magnetic flux density in lateral part and proximity of the end windings, in order to identify the harmonics that characterize each faults for detection and identification. **Chapter seven** presents the experimental obtained from the analysis of the influence of short-circuit fault on the magnetic field in the vicinity of induction motor investigated through the time variation of the output voltage of coil sensors in case of healthy and faulty motor states, for no load motor operation.

CHAPTER 2 FLUX 3D FINITE ELEMENTS MODELS OF THE INDUCTION MOTOR

In this chapter are presented the characteristics of the induction machine used as reference for the 3D finite element models developed using Altair Flux 3D software for the analysis of the fault's detection, evolution and influence on torque, unbalanced force, currents and magnetic field in the proximity of the machine. The induction machine is produced by UMEB and was chosen because has 3 more additional external connections on one phase after first, second and the fourth elementary coils, used to simulate the short-circuit fault. Also, the finite models developed are described for each studied fault and the formulation of the electromagnetic field.

2.1. Description of the induction motor used in the finite element simulations

The induction motor for which the faults are studied, Fig. 2.1, has: 2-pole induction motor; 3-phase star connected; rated-load power, Pn = 7.5 kW; rated source voltage, Unf = 380 V (phase to null value); rated source frequency, f1n = 50 Hz.

This motor has the following main characteristics, Figs. 2.1: The stator armature has 24 slots, The rotor armature has 20 slots. The outer diameter of the stator magnetic core is 212 mm. The inner diameter of the stator is 120 mm. The outer diameter of the rotor is 119 mm; the air-gap thickness is 0.5 mm. The inner diameter of the rotor magnetic core is 40 mm. The length of the stator and rotor magnetic cores is 125 mm.

Fig. 2.2 presents the stator winding. Each phase has 208 turns and 8 elementary coils grouped by 4. The resistance of each phase is 1.54 Ω at 155 ˚C.

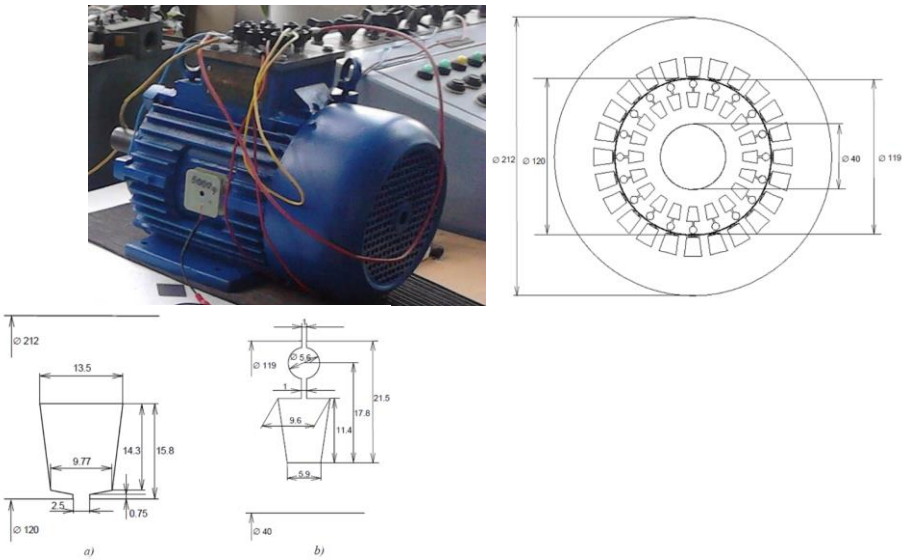

Fig. 2.1. Induction motor used for the study, cross-section of the stator and rotor armatures and Slot dimensions: a) stator slot; b) rotor slot

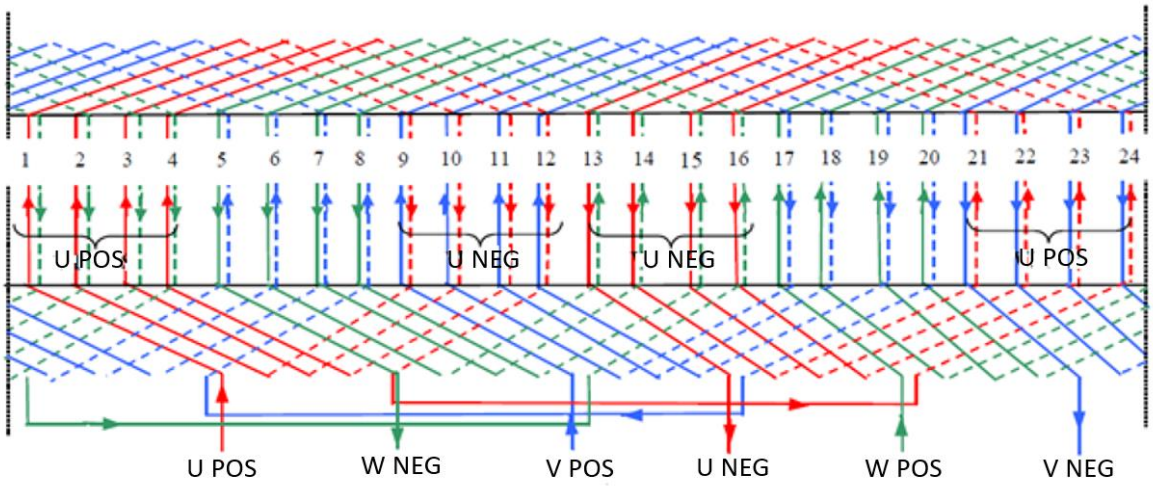

Fig. 2.2. Stator winding

2.2. The induction motor and the 3D finite elements models

This chapter presents the 3D finite element models of the induction motor, Fig. 2.3.

The 3D geometry of the electromagnetic field computation domain, Fig. 2.5. includes: the stator, without frame, and the rotor cores, magnetic nonlinear and nonconductive regions; 24 stator slots; 20 rotor slots, aluminium squirrel-cage with a resistivity of 0.048e-6 Ωm; air gap with 0.5 mm thickness.

The outer diameter of the stator core is 212 mm and the axial length of the magnetic cores is 125 mm. An infinitely extended air region all around the motor is considered.

Fig. 2.3. presents the half of the 3D geometry of the motor where some parts have been made invisible to be able to see the bars of the squirrel-cage and the windings in the stator slots.

The 3D finite element model is coupled with an electric circuit, Fig. 2.4. The circuit contains the three phases of the stator windings. Each phase contains one voltage source and 8 elementary coils. On phase U there is a resistor, R_{SHC}, in parallel with the one elementary coil, U1.

I used the R_{SHC} resistor to simulate the short-circuit between the turns of an elementary coil of phase U, U1 coil, Fig. 2.5.

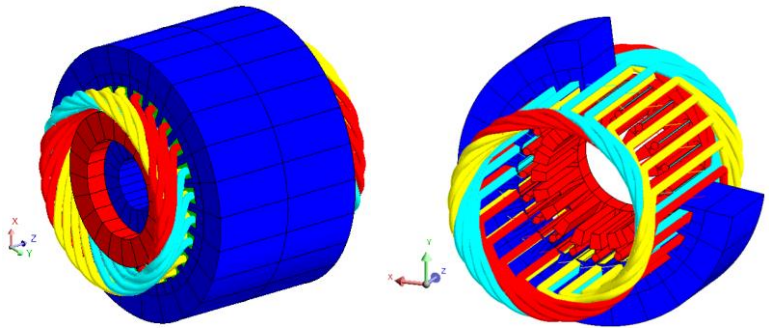

Fig. 2.3. The 3D geometry of the squirrel-cage induction motor

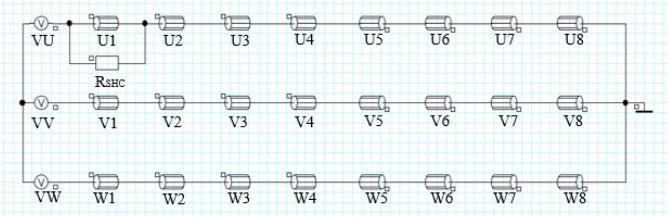

Fig. 2.4. The electrical circuit associated with the finite element model

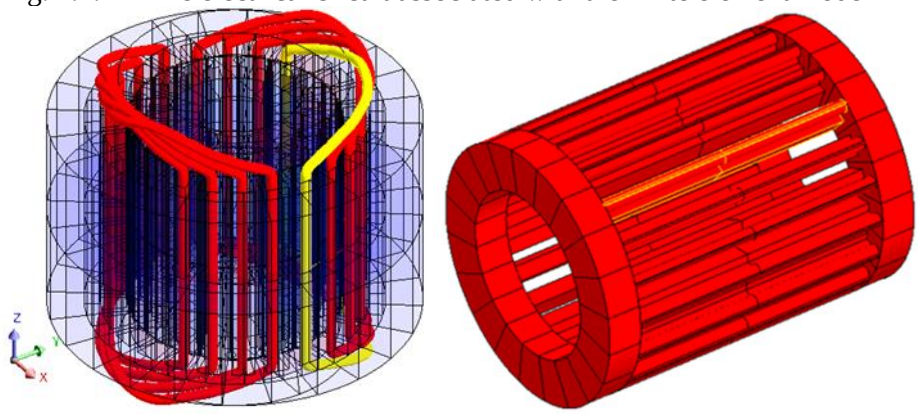

Fig. 2.5. The winding of the phase U, with one elementary coil in short-circuit (yellow) and the squirrel-cage with the bar that will be made broken (yellow)

The studied states of the induction motor are:

- **Healthy (HE):** All bars have the same resistivity, the short-circuit resistor has the value $R_{SHC} = 1$ [MΩ] and the air gap of the motor is uniform;
- **Short-circuit (SHC):** All bars have the same resistivity, the short-circuit resistor has the value $R_{SHC} = 9$ [Ω] and the air gap of the motor is uniform;
- **One Broken Bar (BB)**: All bars have the same resistivity, except one that has 10^7 higher, Fig. 2.5, the short-circuit resistor has the value $R_{SHC} = 1$ [MΩ] and the air gap of the motor is uniform;
- **Static Eccentricity (ECC)**: All bars have the same resistivity, the short-circuit resistor has the value $R_{SHC} = 1$ [MΩ] and a constant non-uniform air gap of the motor, Figure 2.6;
- **Short-circuit and One Broken Bar (SHC&BB)**: All bars have the same resistivity, except one that has 10^7 higher, the short-circuit resistor has the value $R_{SHC} = 9$ [Ω] and the air gap of the motor is uniform;

- **One broken bar and Static Eccentricity (BB&ECC):** All bars have the same resistivity, except one that has 10^7 higher, the short-circuit resistor has the value $R_{SHC} = 1$ [MΩ] and a constant non-uniform air gap of the motor;
- **Static Eccentricity and Short-circuit (ECC&SHC):** All bars have the same resistivity, the short-circuit resistor has the value $R_{SHC} = 9$ [Ω] and a constant non-uniform air gap of the motor;
- **Short-circuit, One Broken Bar and Static Eccentricity (SHC&BB&ECC):** All bars have the same resistivity, except one that has 10^7 higher, the short-circuit resistor has the value $R_{SHC} = 9$ [Ω] and a constant non-uniform air gap of the motor.

During the bar breakage process the value of the current through a bar decrease, the same effect can be obtained through the increasing of the bar resistivity.

Fig. 2.5 presents the squirrel-cage with the bar that will be made broken.

Static eccentricity occurs when the centre line of the rotor is at a constant offset of 0.1 mm, from the centre of the stator that results in a constant non-uniform air-gap, Fig, 2.6.

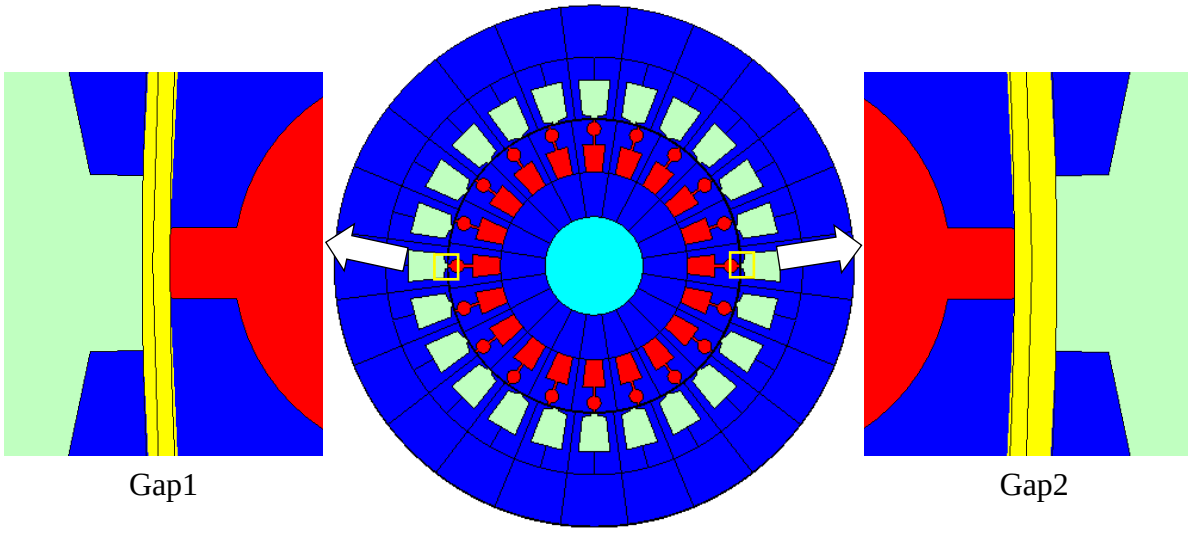

Fig. 2.6. Static eccentricity, Gap1 = 0.4 mm and Gap2 = 0.6 mm

2.3. Formulation of the 3D electromagnetic field in the induction motors

Finite element (FE) in time domain analysis of the squirrel-cage induction motors uses the scalar formulation of the electromagnetic field:

a) Solid conductor type regions: electric vector potential **T** and magnetic scalar potential Φ:

$$\text{curl}\,[\,(1/\sigma)\,\text{curl}\,\mathbf{T}] + \partial[\mu(\mathbf{T} - \text{grad}\Phi)]/\partial t = 0 \qquad (2.1)$$

$$\text{div}[\mu(\mathbf{T} - \text{grad}\Phi)] = 0, \text{ and } \text{div}\mathbf{T} = 0 \qquad (2.2)$$

The current density and the magnetic field intensity: $\mathbf{J} = \text{curl}\,\mathbf{T}$, $\mathbf{H} = \mathbf{T} - \text{grad}\Phi$

b) Magnetic and nonconductive regions: magnetic scalar potential Φ

$$\text{div}[\mu\text{grad}\Phi)] = 0 \qquad (2.3)$$

The magnetic field intensity is $\mathbf{H} = -\text{grad}\Phi$

c) Nonconductive and nonmagnetic regions: reduced magnetic scalar potential Φ_r

$$\text{div}[\mu_0(\mathbf{H}_0 - \text{grad}\Phi_r)] = 0\,, \qquad (2.4)$$

where $\mathbf{H}_0$ - the source magnetic field in the infinitely extended free space, associated to the current density $\mathbf{J}_1$ in the volume V is given by Biot-Savart formula:

$$H_0 = \frac{1}{4\pi}\iiint_V \frac{J_1 \times \mathbf{r}}{r^3} dV \qquad (2.5)$$

The magnetic field intensity is $\mathbf{H} = \mathbf{H}_0 - \text{grad}\Phi_r$

2.4. Step by step in time domain finite element analysis

The finite element time domain analysis of the electromagnetic torque, rotor unbalanced force, phase currents and the electromagnetic field inside and outside the induction motor for known values of the motor voltage supply (3 x 380 V), frequency (50 Hz) and for imposed rotor speed, considers: **2 ms** time step for the **low frequency (LF) analysis**. This value ensures an acceptable accuracy of the step by step in time domain computation of torque and rotor unbalanced force, respectively of their harmonics up to 75 Hz. Harmonics in the range [2 … 74] Hz with a 2 Hz step are computed; **0.05 ms** time step for the **high frequency (HF) analysis**. This ensures an acceptable accuracy of the step by step in time-domain computation of different quantities, respectively of their harmonics up to 1500 Hz. Harmonics in the range [75 … 1500/2000] Hz, with 25 Hz step are computed.

CHAPTER 3 INFLUENCE OF FAULTS ON THE ELECTROMAGNETIC TORQUE

The first step is to see and analyses the influence the individual faults and their combination on electromagnetic torque in rated load motor operation (2880 rpm). The results obtained are presented in this chapter. Some results from this chapter were published on [110].

3.1. Comparison between faulty short-circuit, broken bar, eccentricity states and the healthy state

Table 3.1 present results related to the mean values of the torque and variation with respect HE means values and Table 3.2 the first three harmonics of the torque in decreasing order of the amplitude

Table 3.1 Mean values of the torque and variation with respect of HE mean values

SHC [Nm]	(23.44 + 23.06)/2 = 23.25
BB [Nm]	(15.67 + 16.07)/2 = 15.87
ECC [Nm]	(23.24 + 22.89)/2 = 23.065
HE [Nm]	(23.46 + 23.12)/2 = 23.29
SHC/HE [%]	99.8
BB/HE [%]	68.1
ECC/HE [%]	99.03

The BB fault has the most important influence on the mean value of the rotor torque and the SHC fault has the weakest influence. The decrease of the mean value of the torque is very important in case of the BB fault, around 32 %. This decrease is negligible in case of the SHC and ECC faults.

There is the same harmonic of the torque, with the frequency 850 Hz, which has the highest value of amplitude in the SHC, ECC and HE states.

In the BB fault state, the 4 Hz harmonic has the highest value of amplitude.

Table 3.2 First three harmonics of the torque in decreasing order of the amplitude

	SHC			BB			ECC			HE		
	1	2	3	1	2	3	1	2	3	1	2	3
Amplitude [Nm]	2.04	1.41	1.08	1.44	1.32	0.93	1.90	1.27	1.14	1.89	1.28	1.07
f [Hz]	850	875	1150	4	850	875	850	875	1150	850	875	1150

Frequency groups: {**850** Hz, 875 Hz, 1150 Hz}, **4** Hz

The harmonic of 4 Hz is specific only for the BB fault.

The slotting harmonics of 850 Hz and of 875 Hz are present in all cases HE, SHC, BB and ECC. With these harmonics any of the three faults cannot be detected because they are present also in the healthy state of the motor.

3.2. Double fault states analysis

3.2.1. Comparison between double fault short-circuit and broken bar, one-faults short-circuit and broken bar and the healthy state

The mean value of the torque in the SHC&BB double fault state is 31.91 % lower than that in the SHC fault state, but the difference between values of the mean torque in the SHC&BB double fault state and BB fault state is negligible.

The harmonic of torque with the highest value of the amplitude, 1.44 Nm, in the SHC&BB double fault state with the frequency 4 Hz is different from the similar harmonic in the SHC fault state, with the frequency 850 Hz and the amplitude 2.04 Nm. The most important harmonic in the SHC&BB double fault has the same frequency and amplitude as in the BB fault state.

If the BB fault is superposed on the SHC fault, the mean value of the torque and the amplitude of the most important harmonic of 4 Hz are practically the same as in the case of BB fault.

The weighting of the one-fault BB in the double fault SHC&BB is 99.75 % and the waiting factor of the one-fault SHC in the double fault SHC&BB, 68.09 %, is lower.

Figs 3.1 3.2 and 3.3 presents the aamplitudes of torque LF&HF harmonics, SHC&BB, SHC and BB states,

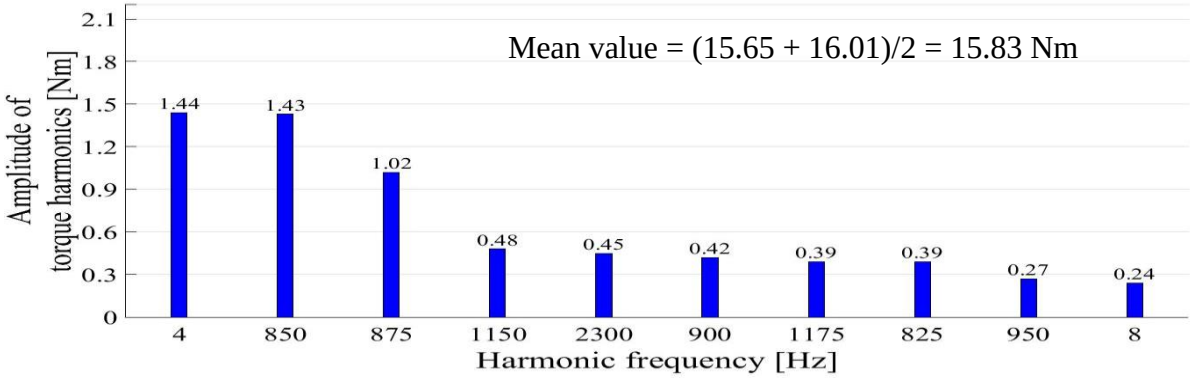

Fig. 3.1. Amplitudes of torque LF&HF harmonics, SHC&BB state

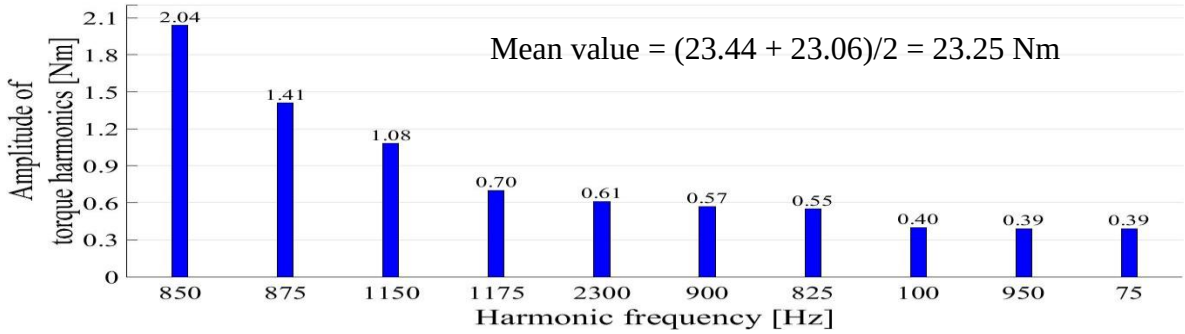

Fig. 3.2. Amplitudes of torque LF&HF harmonics, SHC state

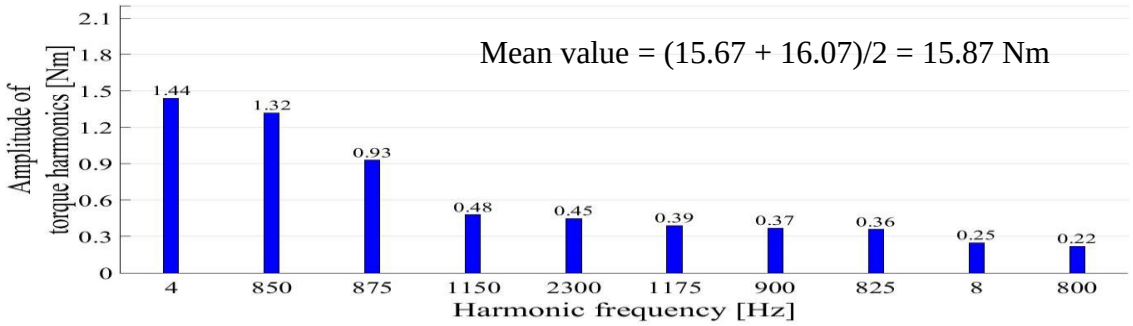

Fig. 3.3. Amplitudes of torque LF&HF harmonics, BB state

3.2.2. Comparison between double fault broken bar and eccentricity, one-faults broken bar and eccentricity and the healthy state

The mean value of the torque in the BB&ECC double fault state is practically the same as in the BB fault state. This vlue is 31.65 % lower than in the ECC fault state.

The harmonic of torque with the highest value of the amplitude, 1.62 Nm, in the BB&ECC double fault state has the frequency 4 Hz, the same as in the BB fault state. This amplitude is (1.62 – 1.44)/1.44 = 12.5 % higher than in the BB fault and (1.90 – 1.62)/1.90 = 14.74 % lower than in the ECC fault.

If the ECC fault is superposed on the BB fault, the mean value of the torque practically doesn't change, but the amplitude of the most important harmonic of 4 Hz increases with 12.5 %.

The weighting of the one-fault BB in the double fault BB&ECC is 99.75 % and the waiting factor of the one-fault ECC in the double fault BB&ECC, 68.09 %, is lower.

3.2.3. Comparison between double fault eccentricity and short-circuit, one-faults eccentricity, short-circuit and the healthy state

The mean value of the torque in the ECC&SHC double fault state is 1.13 % higher than the value for ECC. The difference between the ECC&SHC and SHC values is practically negligible.

The harmonic of torque with the highest value of the amplitude, 2.05 Nm, in the ECC&SHC double fault state has the frequency 850 Hz, the same as in the one-fault ECC and in the one-fault SHC. The amplitude of the 850 Hz harmonic is (2.05 – 1.90)/1.90 = 7.9 % higher in ECC&SHC double fault than in the ECC fault The amplitude of this harmonic is practically the same in the cases ECC&SHC and SHC.

If the SHC fault is superposed on the ECC fault, the mean value of the torque and the amplitude of the most important harmonic of 850 Hz slightly increase.

The weightings of the one-faults ECC and SHC in the double fault ECC&SHC, are practically the same.

3.2.4. Comparison of the short-circuit and broken bar, broken bar and eccentricity, eccentricity and short-circuit double faults, the one-faults short-circuit, broken bar, eccentricity and the healthy state

In the two double faults SHC&BB, BB&ECC the mean value of the rotor torque is almost the same as in the one-fault BB, lower than in double fault ECC&SHC, in one-faults SHC and ECC and in the HE state. As in the SHC fault and in the ECC fault, the mean value of the rotor torque in the double fault ECC&SHC is practically the same as in the HE state.

In the two double faults that include the fault BB, this last fault has a higher weighting factor than the second fault. In the double fault ECC&SHC, the weighting factor of the two faults is practically the same.

The most important harmonic in the double faults SHC&BB and BB&ECC is those of 4 Hz, which is the most important harmonic in the mono BB fault. This harmonic is not important in the ECC&SHC double fault.

The slotting harmonics with the frequency in the group {850 Hz, 875 Hz, 1150 Hz}, has lower, but comparable values of the amplitude. Remember that these harmonics are present also in the HE state. The 850 Hz harmonic is the most important in the ECC&SHC double fault and the second important harmonic in the double faults SHC&BB and BB&ECC.

3.3. Triple fault short-circuit and broken bar and eccentricity state. Comparison between the triple fault SHC&BB&ECC, one-faults short-circuit, broken bar, eccentricity and healthy state

Fig. 3.5 presents the time variation of the torque for SHC&BB&ECC state and in Figs. 3.6. and 3.7 are shown the LF and HF harmonics.

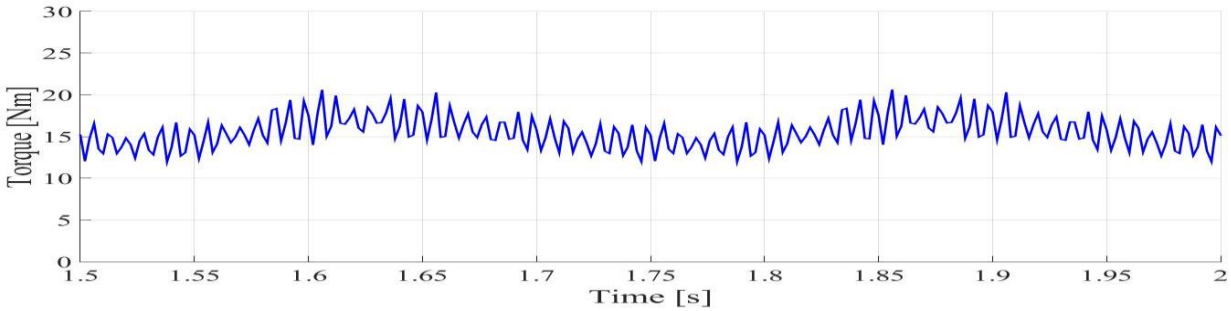

Fig. 3.4. Time variation of the torque for SHC&BB&ECC state. Mean value LF = **15.54 Nm**

In the two triple faults SHC&BB&ECC the mean value of the rotor torque is almost the same as in the one-fault BB, lower than in the one-faults SHC and ECC and in the HE state.

The most important harmonic in the triple faults SHC&BB&ECC is those of 4 Hz, which is the most important harmonic in the mono BB fault.

The slotting harmonics with the frequency in the group {850 Hz, 875 Hz}, has lower, but comparable values of the amplitude. Remember that these harmonics are present also in the HE state.

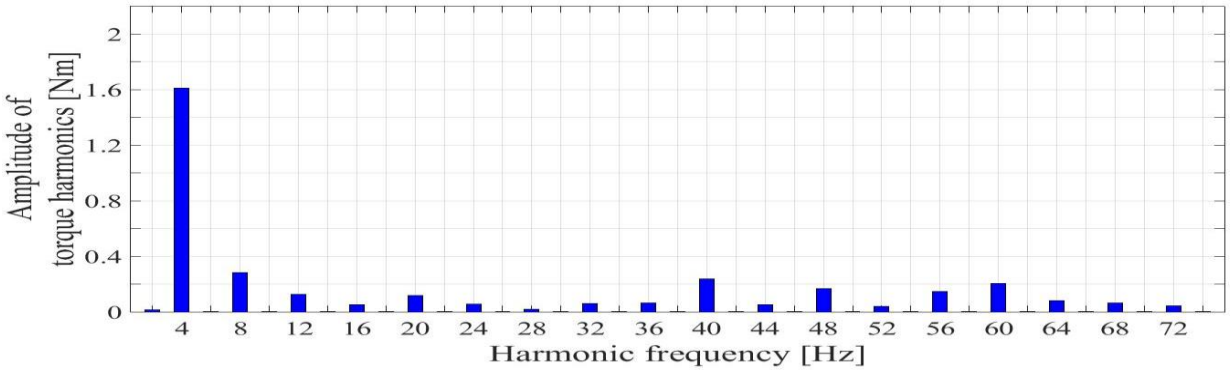

Fig. 3.5. Harmonics LF of the torque for SHC&BB&ECC state

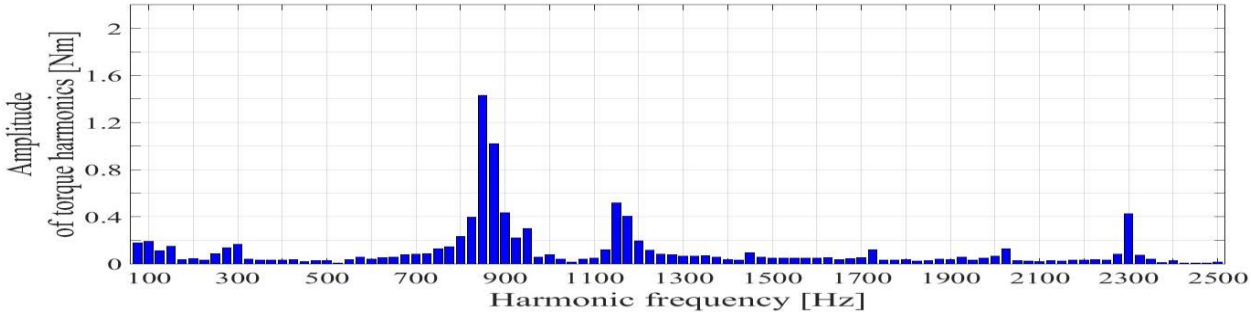

Fig. 3.6. Harmonics HF of the torque for SHC&BB&ECC state

Fig. 3.7.

CHAPTER 4 INLUENCE OF FAULTS ON THE ROTOR UNBALANCED FORCE

The influence of the faults on the rotor unbalanced force is analysed in all motor states for no-load (3000 rpm) and load (2880 rpm) motor operations. Some results from this chapter were published on [110].

4.1. Load motor operation

4.1.1. Comparison between one-faults short-circuit, broken bar, eccentricity and healthy state

The mean values of the rotor unbalanced force and ratios of the mean values is presented in Table 4.1.

Table 4.1 Mean values of the rotor unbalanced force and ratios of the mean values

SHC [N]	(70.87 + 70.41)/2 = 70.64
BB [N]	(368.4 + 383.6)/2 = 376.0
ECC [N]	(197.3 + 191.8)/2 = 194.55
HE [N]	(20.78 + 17.84)/2 = 19.31
SHC/HE	3.660
BB/HE	19.47
ECC/HE	10.08

Order of influence (higher, medium, lower): BB, ECC, SHC

The mean value of the rotor unbalance force presents important or very important increase in the presence of SHC, ECC and BB faults with respect the value in the HE state. In order, this increase is 3.66 times, 10.08 times and 19.47 times.

The order of importance of rotor unbalanced force harmonics reflected in the next table is 4 Hz, the group {40 Hz, 60 Hz} around the supply frequency 50 Hz, the slotting frequencies {1050 Hz, 950 Hz, 1150 Hz} and the group {100 Hz, 200 Hz, 300 Hz} multiplies of 50 Hz.

Table 4.2 First three harmonics of the rotor unbalanced force in decreasing order

	SHC			BB			ECC			HE		
	1	2	3	1	2	3	1	2	3	1	2	3
Amplitude [N]	26.8	25.8	25.5	97.0	23.6	14.2	66.2	49.3	43.7	3.70	3.54	2.14
f [Hz]	200	950	40	4	300	8	60	1050	100	4	1150	8

Frequency groups: **4** Hz, {**60** Hz, 40 Hz}, {**1050** Hz, 950 Hz, 1150 Hz}, {**100** Hz, 200 Hz, 300 Hz}

Table 4.3 First three harmonics of the rotor unbalanced force in decreasing order

	SHC			BB			ECC			HE		
	1	2	3	1	2	3	1	2	3	1	2	3
[%]	37.94	36.52	36.10	25.80	6.277	3.777	34.03	25.34	22.46	19.16	18.33	11.08
f [Hz]	200	950	40	4	300	8	60	1050	100	4	1150	8

4.1.2. Double fault states analysis

4.1.2.1. Comparison between double fault short-circuit and broken bar, one-faults short-circuit and broken bar and the healthy state

In the SHC&BB double fault the harmonic of the rotor unbalanced force with the highest amplitude 86.9 N has the frequency 4 Hz. The same harmonic in the BB state has the amplitude 97.0 N. The next two important harmonics in the SHC&BB double fault, 150 Hz / 52.3 N and 48 Hz / 49.0 N are not important in the BB fault state.

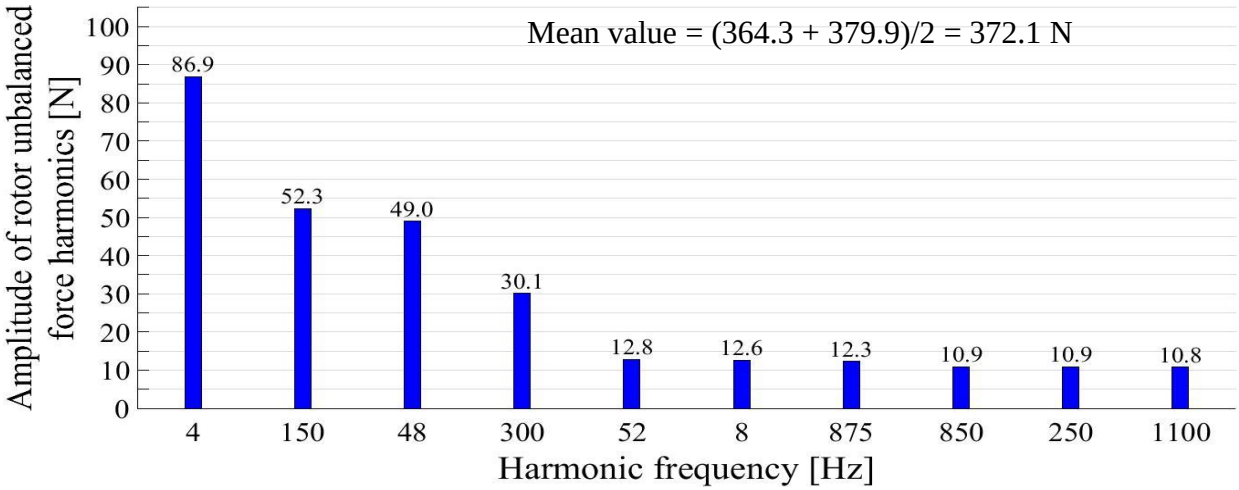

Fig. 4.1. Amplitudes of rotor unbalanced force harmonics, SHC&BB fault state

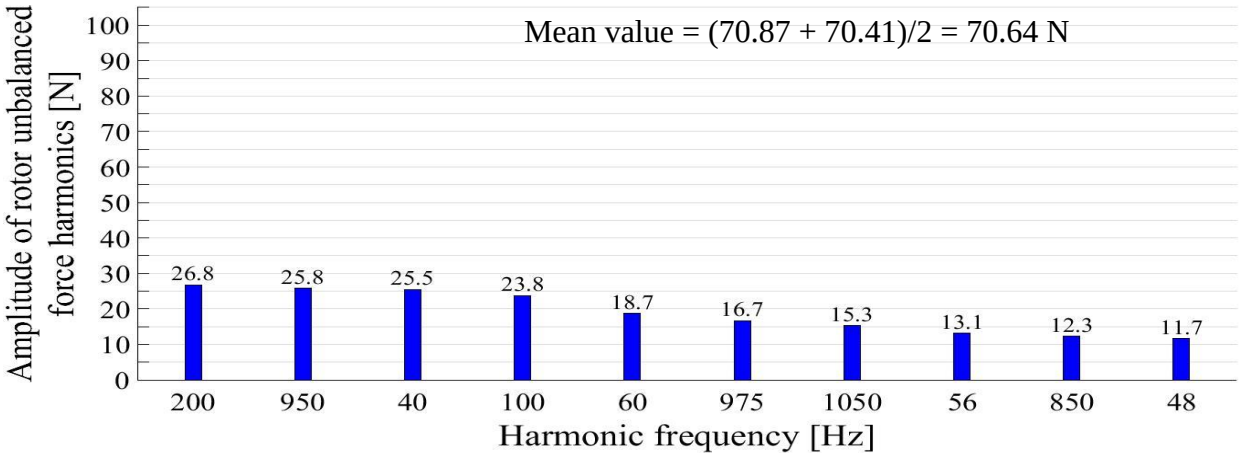

Fig. 4.2. Amplitudes of rotor unbalanced force harmonics, SHC fault state

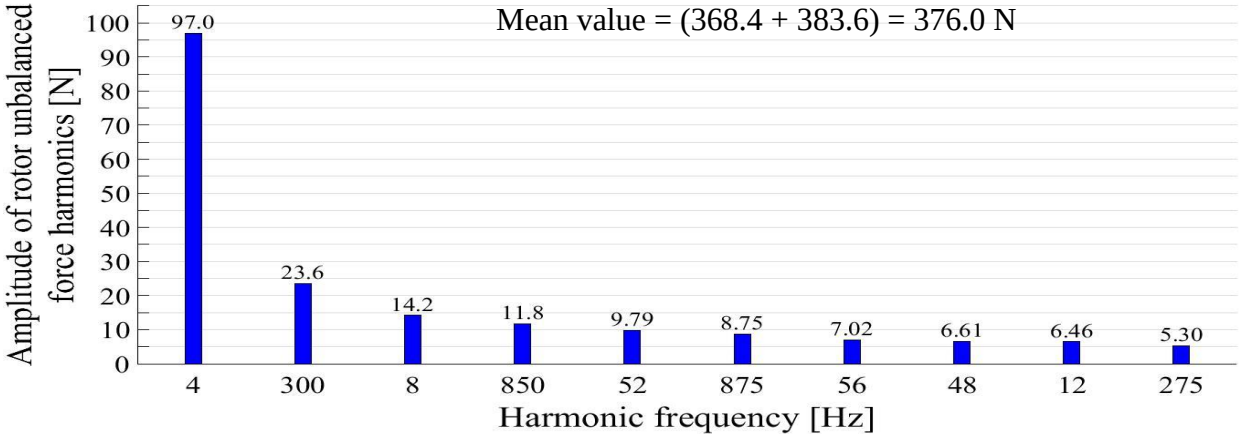

Fig. 4.3. Amplitudes of rotor unbalanced force harmonics, BB state

If the BB fault is superposed on the SHC fault, the mean value of the rotor unbalanced force drastically increases – 5.267 times and the most important harmonics are different. The first important harmonic has the same frequency 4 Hz and the amplitude a little smaller than the most important harmonic in the BB fault state.

The impact of the one-fault BB in the double fault SHC&BB, 101.05 %, is much higher than the impact of the SHC fault, which is only 18.98 %.

4.1.2.2. Comparison between double fault broken bar and eccentricity, one-faults broken bar and eccentricity and the healthy state

The mean value of the rotor unbalanced force in BB&ECC state is 1.5% higher than that in BB state and 95% higher than that from ECC state.

The mean value of the rotor unbalanced force in the BB&ECC double fault state is slightly higher than in the BB fault state and 387.05 N / 194.55 N = 1.989 times higher than in the ECC fault state.

In the BB&ECC double fault the harmonic of the rotor unbalanced force with the highest amplitude 149 N has the frequency 48 Hz. This harmonic it is not important in the BB fault and ECC fault states.

The second important harmonic in the BB&ECC double fault, 4 Hz / 105 N, has a little higher amplitude than the similar harmonic 4 Hz / 97 N in the BB fault state.

If the ECC fault is superposed on the BB fault, the mean value of the rotor unbalanced force slightly increases, from 376.0 N at 387.05 N. A new most important harmonic, 48 Hz / 149 N, takes the place of the first important harmonic of 4 Hz in the BB fault state. The harmonic of 4 Hz becomes the second important harmonic in the BB&ECC double fault

The impact of the one-fault BB in the double fault BB&ECC, 97.1 %, is higher than the impact of the ECC fault, which is 50.3 %.

4.1.2.3. Comparison between double fault eccentricity and short-circuit, one-faults eccentricity, short-circuit and the healthy state

The mean value of the rotor unbalanced force in the ECC&SHC double fault state, 170.3 N, is lower than in the ECC fault state, 195.55 N, and 170.2 N / 70.64 N = 2.409 times higher than in the SHC fault state.

In the ECC&SHC double fault the harmonic of the rotor unbalanced force with the highest amplitude 87.8 N has the frequency 100 Hz. This harmonic has smallest values in the ECC fault state, 43.7 N, and 23.8 N in the SHC fault state.

The second important harmonic in the ECC&SHC double fault, 60 Hz / 77.4 N, has a little higher amplitude than the similar and most important harmonic 60 Hz / 66.2 N in the ECC fault state.

If the SHC fault is superposed on the ECC fault, the mean value of the rotor unbalanced force decreases from 194.55 N at 170.3 N. A new most important harmonic, 100 Hz / 87.8 N, takes the place of the first important harmonic, 60 Hz / 66.2 N in the ECC fault state. The harmonic of 60 Hz, with amplitude increases at 77.4 N becomes the second important harmonic in the ECC&SHC double fault state.

The impact of the one-fault ECC in the double fault ECC&SHC, 114.24 %, is higher than the impact of the SHC fault, which is 41.48 %.

4.1.2.4. Comparison of the short-circuit and broken bar, broken bar and eccentricity, eccentricity and short-circuit double faults, the one-faults short-circuit, broken bar, eccentricity and the healthy state

In the two double faults SHC&BB, BB&ECC the mean value of the rotor unbalanced force is almost the same as in the one-fault BB, higher than in the double fault ECC&SHC, in the one-faults SHC and ECC and in the HE state. The rotor unbalanced force in the double fault ECC&SHC, 170.3 N, is a little lower than 194.55 N in the ECC fault and higher than 70.64 N in the SHC fault.

All forces in the double fault states SHC&BB, BB&ECC and ECC&SHC are much higher than in the HE state. These forces are also more or less higher than in the one-faults states SHC, BB and ECC.

The impact of the BB fault is the more important in the BB&ECC fault compared with the ECC fault impact, are much more important in the SHC&BB fault.

The most important harmonic of the rotor unbalanced force in the double fault SHC&BB is those of 4 Hz, which is the most important harmonic in the mono BB fault. The second important

harmonic in the BB&ECC fault, with the frequency 4 Hz has the amplitude higher than in the SHC&BB fault.

The most important harmonic of the rotor unbalanced force in the double fault BB&ECC has the frequency 48 Hz, which belongs to a group of frequencies around the supply frequency 50 Hz. To the same group belong the second important harmonic 60 Hz / 77.4 N of the ECC&SHC fault and the third important harmonic 48 Hz / 49.0 N of the SHC&BB fault.

The most important harmonic of the rotor unbalanced force in the double fault ECC&SHC, 100 Hz / 87.8 N and the second important harmonic of the SHC&BB fault belong to a group of frequencies multiply of 50 Hz.

There are also present slotting harmonics, the 1100 Hz / 46.1 N in the BB&ECC fault and 1050 Hz / 53.4 N in the ECC&SHC fault.

4.1.3. Triple fault short-circuit and broken bar and eccentricity state analysis

Fig. 4.4 Presents the time variations of the rotor unbalanced force, SHC&BB&ECC state. Mean value LF = 363.5 N. The amplitudes harmonics of the rotor unbalanced force a re shown in Figs 4.5 and 4.6 for LF and HF.

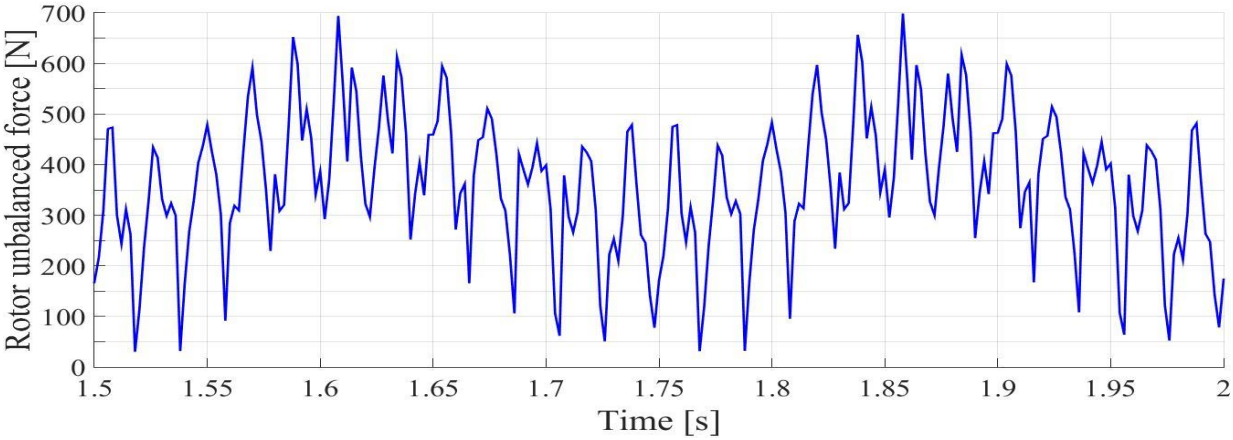

Fig. 4.4. Time variation of the rotor unbalanced force, SHC&BB&ECC state.

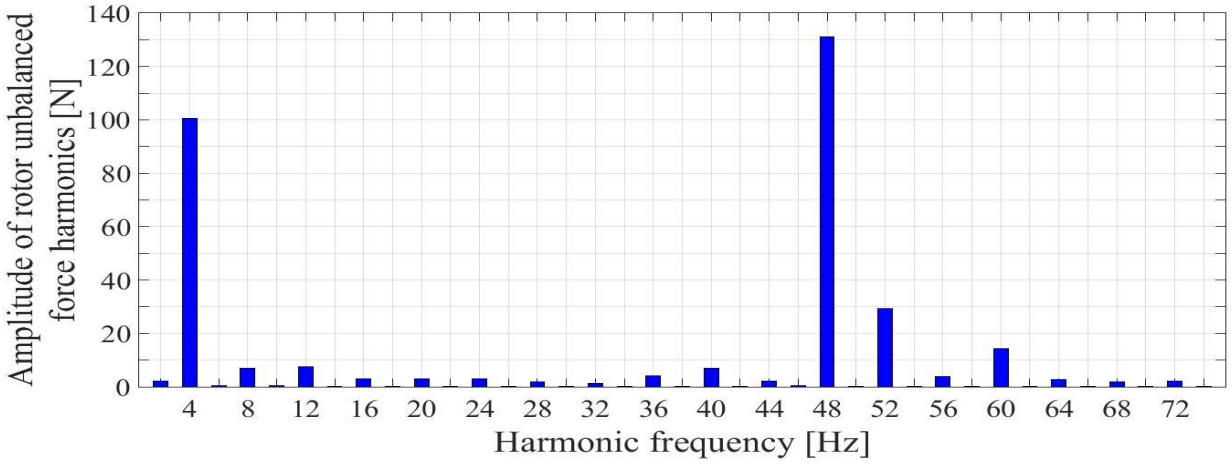

Fig. 4.5. Harmonics LF of the rotor unbalanced force, SHC&BB&ECC state

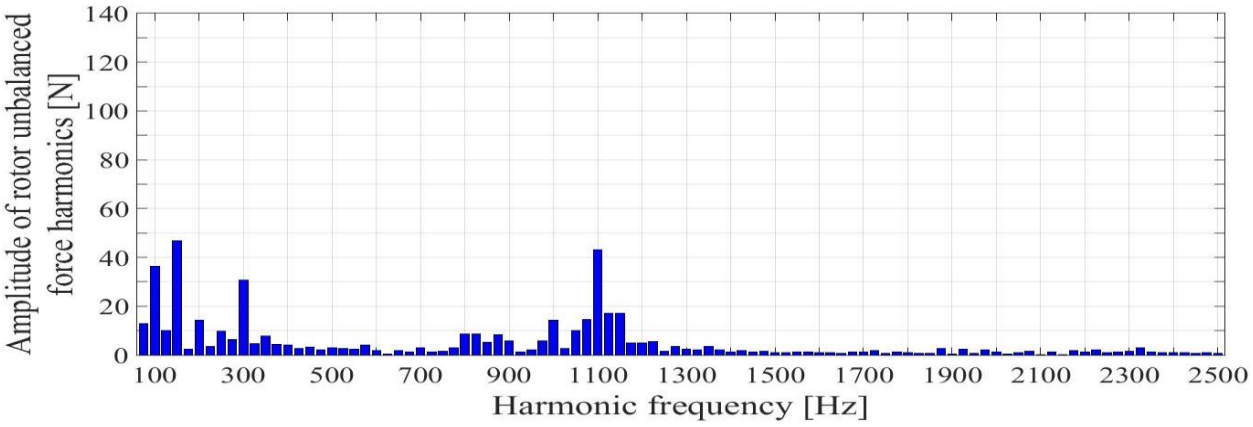

Fig. 4.6. Harmonics HF of the rotor unbalanced force, SHC&BB&ECC state

4.3.2. Comparison between triple fault short-circuit and broken bar and eccentricity state. one-faults short-circuit, broken bar, eccentricity and healthy state

In the triple fault SHC&BB&ECC the mean value of the rotor unbalanced force is almost the same as in the one-fault BB, higher than in the one-faults ECC and SHC and much higher than in the HE state.

The impact of the BB fault is the more important in the triple SHC&BB&ECC fault compared with ECC and SHC faults.

The harmonic 48 Hz / 131 N and 4 Hz / 101 N are the first two important harmonics of the rotor unbalanced force in the triple SHC&BB&ECC fault. The amplitudes of the next two harmonics in order of importance, 150 Hz / 46.7 N and 1100 Hz / 43.1 N, are not much lower.

4.2. No-load motor operation

4.2.1. Comparison between one-faults short-circuit, broken bar, eccentricity and healthy state

The mean value of the rotor unbalanced force presents low, important and very important increase in the presence of BB, SHC and ECC faults with respect the value in the HE state. In order, this increase is 1.375 times, 11.39 times and 19.10 times.

The order of importance of rotor unbalanced force harmonics reflected in the next table is group {100 Hz, 200 Hz, 300 Hz, 600 Hz} multiplies of 50 Hz, the slotting frequencies {1100 Hz, 1200 Hz, 900 Hz } and the 56 Hz around the supply frequency 50 Hz.

4.2.2. Double fault states analysis

4.2.2.1. Comparison between double fault short-circuit and broken bar, one-faults short-circuit and broken bar and the healthy state

The mean value of the rotor unbalanced force in SHC&BB double fault state is 75.04/8.559 = 8.767 times higher than in the BB state and slightly higher than in the SHC fault state, 5.809 %.

In the SHC&BB double fault the harmonic of the rotor unbalanced force with the highest amplitude 35.4 N has the frequency 100 Hz. The same harmonic in the SHC state has the amplitude 37.5 N. The next important harmonics in the SHC&BB double fault is 200 Hz / 19.1 N is not important in the BB fault state.

If the BB fault is superposed on the SHC fault, the mean value of the rotor unbalanced force slightly increases – 5.809 % and the most important harmonics are the same.

The impact of the one-fault SHC in the double fault SHC&BB, 94.51 %, is much higher than the impact of the BB fault, which is only 11.41 %.

4.2.2.2. Comparison between double fault broken bar and eccentricity, one-faults broken bar and eccentricity and the healthy state

The mean value of the rotor unbalanced force in the BB&ECC double fault state is slightly higher than in the ECC fault state and 123.0 N / 8.559 N = 14.37 times higher than in the BB fault state.

In the BB&ECC double fault the harmonic of the rotor unbalanced force with the highest amplitude 26.9 N has the frequency 1100 Hz. This harmonic it is the important in the ECC fault.

The second important harmonic in the BB&ECC double fault, 100 Hz / 23.1 N, has a little higher amplitude than the similar harmonic 100 Hz / 21.0 N in the ECC fault state.

If the ECC fault is superposed on the BB fault, the mean value of the rotor unbalanced force highly increases, from 8.559 N at 123.0 N. A new most important harmonic, 1100 Hz / 26.9 N, takes the place of the first important harmonic of 300 Hz in the BB fault state. The harmonic of 300 Hz it is not one of the most important harmonics in the BB&ECC double fault.

The impact of the one-fault ECC in the double fault BB&ECC, 96.67 %, is much higher than the impact of the BB fault, which is 6.959 %.

4.2.3.3. Comparison between double fault eccentricity and short-circuit, one-faults eccentricity, short-circuit and the healthy state

The mean value of the rotor unbalanced force in the ECC&SHC double fault state, 93.13 N, is lower than in the ECC fault state, 118.9 N, and 93.13 N / 70.92 N = 1.313 times higher than in the SHC fault state.

In the ECC&SHC double fault the harmonic of the rotor unbalanced force with the highest amplitude 40.3 N has the frequency 100 Hz. This harmonic has 21.0 N in the ECC fault state and 37.5 N in the SHC fault state.

The second important harmonic in the ECC&SHC double fault, 1100 Hz / 15.7 N, has a lower amplitude than the similar and most important harmonic 1100 Hz / 26.9 N in the ECC fault state and higher amplitude, 1100 Hz / 11.9 N in SHC fault.

If the SHC fault is superposed on the ECC fault, the mean value of the rotor unbalanced force decreases from 118.9 N at 93.13 N. A new most important harmonic, 100 Hz / 40.3 N, takes the place of the first important harmonic, 1100 Hz / 26.9 N in the ECC fault state. The harmonic of 1100 Hz, with an amplitude that decreases at 15.7 N, becomes the second important harmonic in the ECC&SHC double fault state.

If the ECC fault is superposed on the SHC fault, the mean value of the rotor unbalanced force increases from 70.92 N at 93.13 N. The most important harmonic, 100 Hz / 40.3 N, has a slightly higher amplitude, 37.5 N in SHC. The harmonic of 1100 Hz, with an amplitude that increases at 15.7 N, becomes the second important harmonic in the ECC&SHC double fault state.

The impact of the one-fault ECC in the double fault ECC&SHC, 127.7 %, is higher than the impact of the SHC fault, which is 76.15 %.

4.2.3.4. Comparison of the short-circuit and broken bar, broken bar and eccentricity, eccentricity and short-circuit double faults, the one-faults short-circuit, broken bar, eccentricity and the healthy state

In the three double faults SHC&BB, BB&ECC and ECC& SHC the mean value of the rotor unbalanced force has different values than that in mono states.

The rotor unbalanced force in the double fault BB&ECC, 123.0 N, is a little higher than 118.9 N in the ECC fault and much higher than 5.559 N in the BB fault.

All forces in the double fault states SHC&BB, BB&ECC and ECC&SHC are much higher than in the HE state. These forces are also higher than in the BB one-fault state.

The impact of the ECC fault is the most important in the BB&ECC fault compared with the BB fault impact and the most important in the ECC&SHC fault compared with the SHC fault impact

The impact of the SHC fault is the most important in the SHC&BB fault compared with the BB fault impact.

The most important harmonic of the rotor unbalanced force in the double fault SHC&BB is that of 100 Hz, which is the most important harmonic in the mono SHC fault and in the most double fault ECC&SHC, with little higher value of amplitude.

The second harmonic in the double fault SHC&BB is 200 Hz, that is third harmonic in ECC&SHC fault, with a lower amplitude.

The second important harmonic in the BB&ECC fault, with the frequency 100 Hz has the amplitude lower than in the SHC&BB fault.

The most important harmonic of the rotor unbalanced force in the double fault BB&ECC has the frequency 1100 Hz, which belongs to a group of slotting frequencies.

The second important harmonic in the ECC&SHC fault, with the frequency 1100 Hz has the amplitude higher than in the SHC&BB fault, where is the third harmonic, and lower than that in BB&ECC double fault.

The third harmonic in BB&ECC double fault is the 1200 Hz, which is not present among the first three harmonics of the other double faults.

4.2.3. Comparison between triple fault short-circuit and broken bar and eccentricity state. one-faults short-circuit, broken bar, eccentricity and healthy state

In the triple fault SHC&BB&ECC the mean value of the rotor unbalanced force is higher than the in the one-fault SH, much higher than in the one-faults BB, lower than that in ECC state and much higher than in the HE state.

The impact of the ECC fault is the most important in the triple SHC&BB&ECC fault compared with SHC and BB faults.

The harmonic 100 Hz / 40.7 N is the most important harmonic of the rotor unbalanced force in the triple SHC&BB&ECC fault. The amplitudes of the next two harmonics in order of importance, 1100 Hz / 15.7 N and 200 Hz / 12.3 N, are not much lower.

CHAPTER 5 DETECTION OF FAULTS THROUGH THE STATOR CURRENTS

This chapter presents results related to the detection of mono and multiple faults in a squirrel-cage induction motor through theirs influence on the harmonics of the stator currents in load (2880 rpm) and no-load (3000 rpm) motor operations.

The criterion based on which the faults influence is evaluated:

$$\boldsymbol{Efficiency\ in\ fault\ detection} = \frac{value\ of\ harmonic\ amplitude\ in\ faulty\ state}{value\ of\ harmonic\ amplitude\ in\ healthy\ state} = \frac{FA}{HE} \quad (5.1)$$

The results corresponding to the load motor operation. Some of the results are presented in paper [111].

5.1. Detection of one-fault states in load motor operation

The influence of mono-fault states on the stator currents is presented in this part.

Figs. 5.1, 5.2 and 5.3 presents the time variation of the phase currents for the one-faults and healthy state. There is visible difference of the time variation of the currents in BB state from the other states for all currents and a small difference in case of SHC state from the ECC and HE states only for the IU current, the short-circuited coil is on U phase.

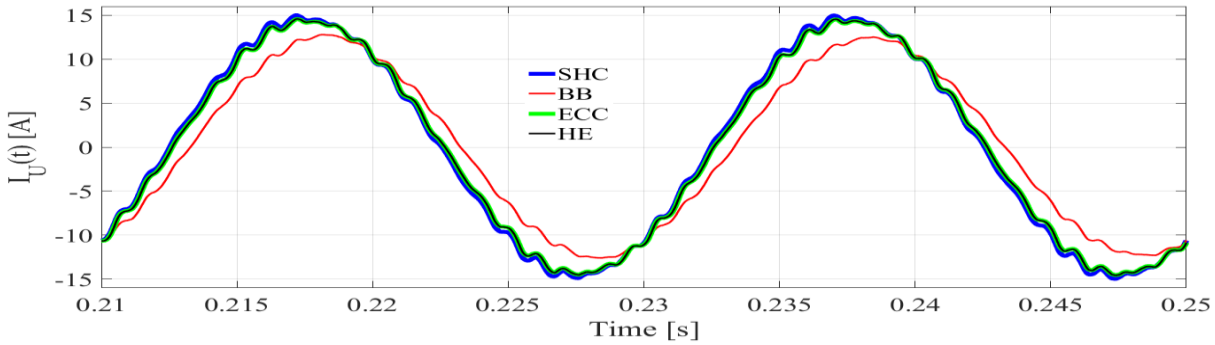

Fig. 5.1. Time variation of the I_U current in SHC, BB, ECC and HE states, load operation

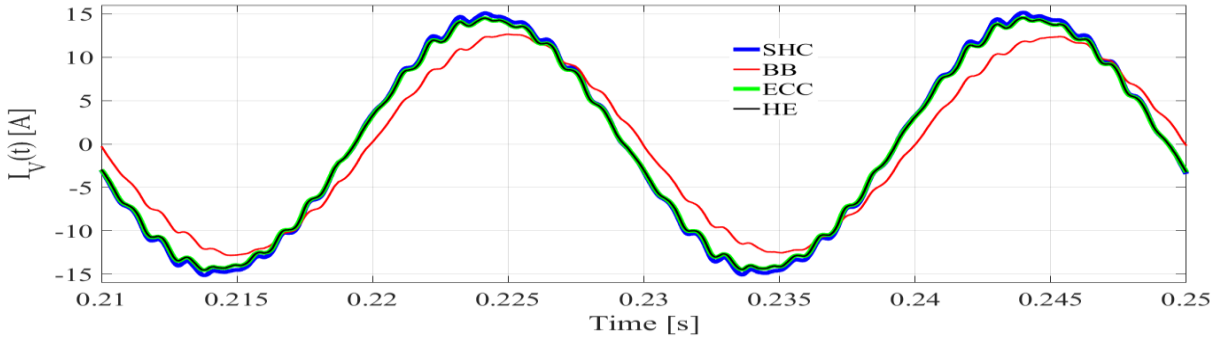

Fig. 5.2. Time variation of the I_V current in SHC, BB, ECC and HE states, load operation

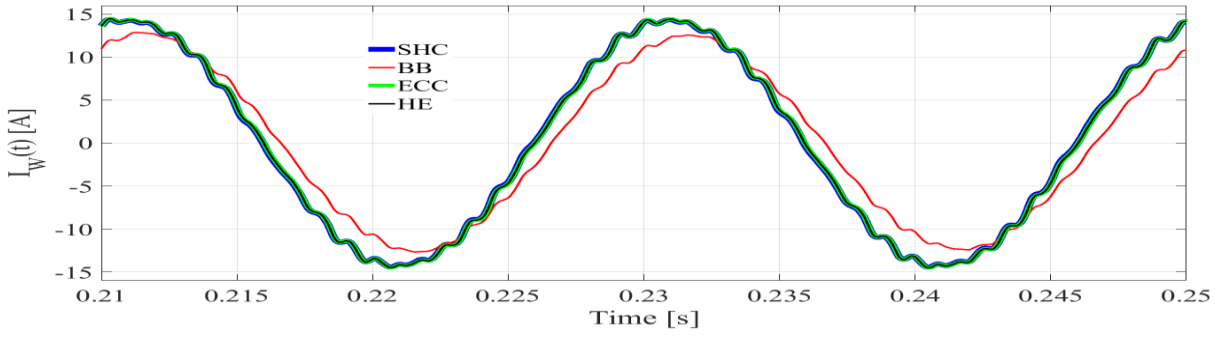

Fig. 5.3. Time variation of the I_W current in SHC, BB, ECC and HE states, load operation

Table 5.1 presents information about the stator currents in the mono-fault states and HE state. The information presented are the RMS, mean values and the unbalance of the phase currents, current unbalanced.

The mean value of the currents in the three phases is: $I_m = \frac{I_U+I_V+I_W}{3}$ (5.2)

The current unbalance is calculated in terms of maximum deviation of current in a phase from the mean value of the currents of the three phases.

The formula used to calculate the percentage deviation is:

$$\frac{Max(|I_m-I_U|,|I_m-I_V|,|I_m-I_W|)}{I_m} \times 100 \quad (5.3)$$

In SHC state the unbalance of the phase currents is much higher than that in HE state.

The rms value of the currents are lower in case of BB fault and almost the same as those in HE when the ECC fault is present. I_U

Table 5.1 Information about the three phase currents in SHC, BB, ECC and HE states, load

State	I_U [A]	I_V [A]	I_W [A]	I_m [A]	Current unbalance [%]
HE	10.162	10.153	10.143	10.153	0.09521
SHC	10.373	10.502	10.119	10.331	2.0552
BB	8.8022	8.8212	8.8146	8.8127	0.1188
ECC	10.135	10.151	10.146	10.144	0.08872

Table 5.2 Currents and Power through/in U1 and R_{SHC}, SHC state, load motor operation

State	I_{U1} [A]	P_{U1} [W]	I_{RSHC} [A]	P_{RSHC} [W]
SHC	9.3660	16.887	5.4755	269.83

In SHC state the I_{U1} current is 9.3660 A, lower than that from HE state, 10.162 A, and the I_U current, 10.373 A, Tables 5.1 and 5.2.

The power in the R_{SHC} resistor is 269.83 W, much higher than in the U1 coil, 16.887 W, SHC state.

5 1.1. Detection of mono-fault states through harmonics of I_U current

The values of the efficiency in mono-fault states detection are presented in the next three figures for low-frequency (LF - [2 - 74] Hz) and high-frequency (HF- [75 - 750] Hz and [775 - 1500] Hz) harmonics of I_U current.

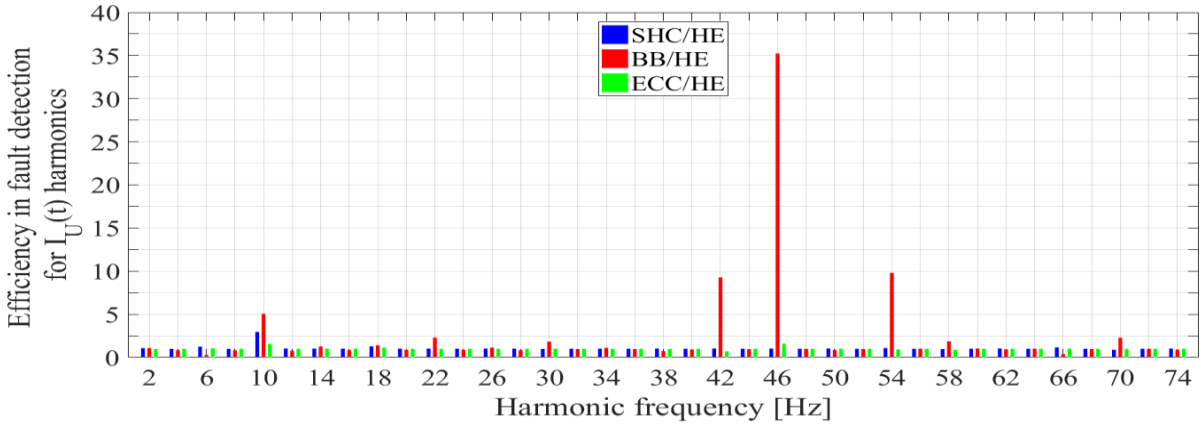

Fig. 5.4. Efficiency in the SHC, BB and ECC states detection through LF I_U current harmonics, load operation

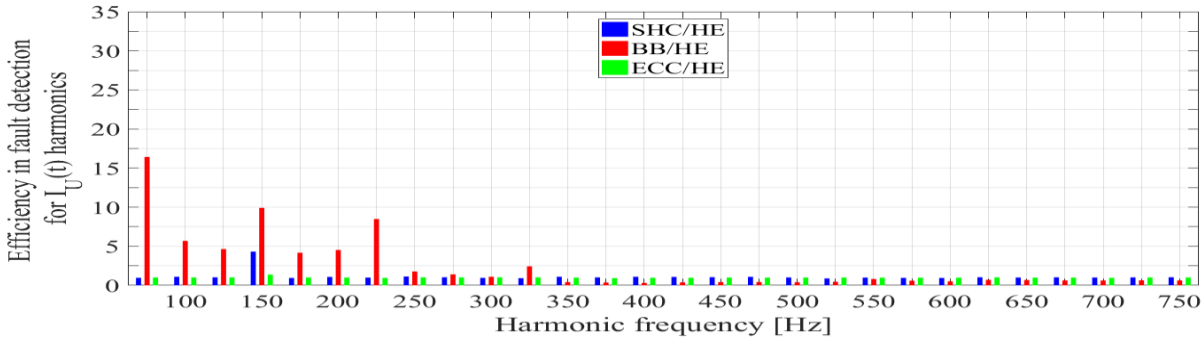

Fig. 5.5. Efficiency in the SHC, BB and ECC states detection through HF I_U current harmonics in the range [75 - 750] Hz, load operation

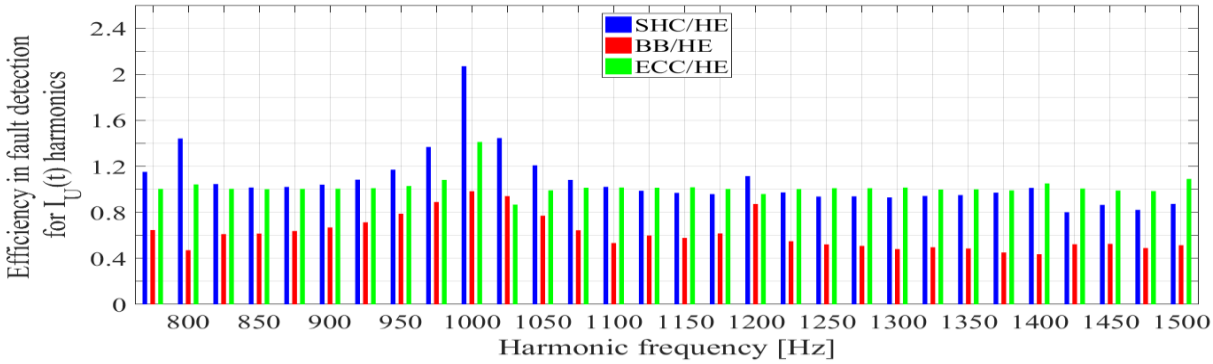

Fig. 5.6. Efficiency in the SHC, BB and ECC states detection through HF I_U current harmonics in the range [775 - 1500] Hz, load operation

Table 5.3 highlights the first three harmonics with the highest values of the efficiency in fault detection for I_U current.

The harmonics are grouped depending on the type:

- harmonics multiple of the frequency of the rotor currents, 2 Hz;
- harmonics around the supply frequency, 50 Hz;
- harmonics multiple of the supply frequency and multiple of 25 Hz;
- slot harmonics, higher than 500 Hz.

Table 5.3 The first three harmonics of I_U with the highest values of efficiency in mono-fault detection, load motor operation

State	SHC			BB			ECC		
Order	1	2	3	1	2	3	1	2	3
f [Hz]	150	10	1000	46	75	150	46	10	1000
FA [mA]	11.12	16.47	33.80	492.2	72.7	25.53	22.07	8.774	23.05
HE [mA]	2.576	5.588	16.33	13.97	4.427	2.576	13.97	5.588	16.33
FA/HE	4.317	2.947	2.070	35.23	16.42	9.911	1.580	1.570	1.412

Frequency groups: 10 Hz, 46 Hz, {75 Hz, 150 Hz}, 1000 Hz

The ECC fault has the smallest influence on the harmonics of the current and the BB state has the highest in fluence.

The highest value of efficiency, 35.23, is for 46 Hz harmonic in BB state, Table 5.3.

In SHC state the harmonic with the highest efficiency, 4.317, is 150 Hz, different from that in BB state, consequently the SHC and BB faults can be differentiated.

In ECC state there is the same harmonic with the highest efficiency as in BB state, but the second harmonics are different, 75 Hz vs. 10 Hz, consequently the ECC fault and BB fault can be differentiated.

Through the harmonics of the I_U current can be detected if a fault is SHC, BB or ECC.

5.1.2. Detection of mono-fault states through harmonics of I_V current

Figures 5.7, 5,8 and 5.9 shows the efficiency in the one-faults detection through LF and HF harmonics of I_V current.

The first three harmonics of I_V current with the highest values of efficiency in one-fault detection are shown in next table.

The 75 Hz harmonic has the highest efficiency in fault detection, 30.84, in BB state, Table 5.4.

In SHC state the harmonic with the highest efficiency, 14.52, is 150 Hz, different from that in BB state, consequently the SHC and BB fault can be differentiated.

The first harmonic in ECC state is the same as in SHC state, 150 Hz, but the second and the third ones are different,75 Hz and 275 Hz vs 1000 Hz and 1225 Hz, therefor the ECC and SHC fault can be differentiated.

Through the harmonics of the I_V current the SHC, BB and ECC one-faults can be detected.

5.1.3. Detection of mono-fault states through harmonics of I_W current

The highest efficiency, 34.35, is for 75 Hz harmonic in BB state, Table 5.5.

The 150 Hz harmonic has the highest efficiency is fault detection, 6.896, for SHC state and is different from that in BB state, 75 Hz, consequently the SHC and BB fault can be differentiated.

In ECC state the highest efficiency is 1.170 for 6 Hz harmonics of the I_W current, that is different from the ones from SHC and BB states, therefor the ECC fault can be detected.

Through the harmonics of the I_W current can be detected if a fault is SHC, BB or ECC.

5.2. Study of double-fault states detection

This part presents the study of double-fault detection based on the harmonics of the phase currents.

In SHC&BB state the rms values of the phase currents are lower than in healthy state, as in BB state, and the unbalance of the currents is higher, as in SHC state, Table 5.4.

The BB&ECC state is characterized by lower rms values of the currents.

In ECC&SHC state the current presents a higher value of unbalance than in healthy state, as in the SHC state.

Table 5.4 Information about the three phase currents in SHC&BB, BB&ECC, ECC&SHC, SHC, BB, ECC and HE states, load motor operation

State	I_U [A]	I_V [A]	I_W [A]	I_m [A]	Current unbalance [%]
SHC&BB	8.9237	9.1518	8.7739	8.9498	2.2570
BB&ECC	8.7900	8.8258	8.8271	8.8143	0.2757
ECC&SHC	10.343	10.496	10.123	10.321	1.9153

Table 5.5 Currents and Power through/in U1 and R_{SHC}, SHC&BB, ECC&SHC and SHC states, load motor operation

State	I_{U1} [A]	P_{U1} [W]	$I_{R_{SHC}}$ [A]	$P_{R_{SHC}}$ [W]
SHC&BB	9.1530	16.127	5.4210	264.49
ECC&SHC	9.3656	16.885	5.4504	267.37
SHC	9.3660	16.887	5.4755	269.83

The value of the I_{U1} current in SHC&BB state is 9.1530 A, lower than the values from ECC&SHC and SHC states.

The values of I_{U1} current is higher than the I_U current in SHC&BB state and lower than I_U current in ECC&SHC and SHC states, Tables 5.4 and 5.5.

The power in the R_{SHC} resistor is 264.49 W in SHC&BB state, slightly lower than that in ECC&SHC or SHC state. The power in R_{SHC} resistor is much higher than in the U1 coil for each state that presents the SHC fault, Table 5.7.

5.2.1. Detection of double-fault states through harmonics of I_U current

The first two harmonics of the I_U current are the same for SHC&BB and BB&ECC, but the third is different, 150 Hz and 54 Hz, consequently the two states can be differentiated.

In ECC&SHC state the 150 Hz harmonic has the highest value of efficiency, different from those in SHC&BB and BB&ECC states, therefore the ECC&SHC state can be differentiated from the other double-faults.

The first three harmonics of I_U current with the highest values of efficiency if fault detection for SHC&BB and BB states are the same, but the value of efficiency in fault detection for 150 Hz harmonic is 68.5 % higher than that in BB state, consequently the two states can be differentiated if the value from the BB state are known.

When the BB fault is present in a fault state the first two harmonics based on the efficiency criterion are 46 Hz and 75 Hz.

In ECC&SHC state the first three I_U current are the same as in SHC, but the values of deficiency are 19.1 %, 15.6 % and 18.0% higher, therefor the double fault can be differentiated from the mono-fault if the values of the efficiency in one-faults are known.

Through I_U harmonics the double-faults states can be detected if the first three harmonics and their efficiency in one-faults detection are known.

5.2.2. Detection of double-fault states through harmonics of I_V current

The first three harmonics with the highest value of the efficiency in double-fault detection are the same for SHC&BB and BB&ECC states, consequently the two states cannot be differentiated if the mono-fault harmonics and their efficiencies are not known.

In the ECC&SHC state the first three harmonics are different from those in SHC&BB and BB&ECC, consequently the ECC&SHC state can be differentiated from the others double-faults.

The first two harmonics in the ECC&SHC state are the same as in SHC state, but the 150 Hz harmonics has a 2.89 times higher efficiency in case of the double-fault, therefor the ECC&SHC state can be detected and differentiated, if the information related with the mono-fault are known.

If the first three harmonics and their efficiency in fault detection corresponding to the mono-fault are known the double-faults states can be detected and differentiated through I_U current harmonics.

5.2.3. Detection of double-fault states through harmonics of I_W current

The first three harmonics of the I_W current with the highest value of the efficiency in fault detection are the same, 75 Hz, 225 Hz and 46 Hz, for SHC&BB, BB&ECC and BB states.

If the BB fault occurs after the SHC fault, the SHC&BB double0-fault can be detected and differentiated from the one-faults and ECC&SHC double-fault.

Also, if the BB fault occurs after the ECC fault, the BB&ECC fault can be detected and differentiated from the one-faults and ECC&SHC double-fault.\

But if the SHC or ECC faults occurs after the BB fault is already present, the SHC&BB and BB&ECC can not be detected as double-faults and can not be differentiated from the BB fault.

The ECC&SHC state is characterized by: the same first harmonic as SHC state, 150 Hz; the second harmonic is the first in ECC state, 6 Hz; the third harmonic as SHC state, 250 Hz; different harmonics from the other two double-fault states. Therefor this double-fault state can be differentiated from the one-faults and double-faults only if the first three harmonics of the one-faults are known.

5.3. Study of the triple-fault state detection

In this section presents results related to the study on the detection of the triple-fault state.

In the SHC&BB&ECC state the rms values of the phase currents are lower than those in healthy state, almost the same as in SHC&BB, and slightly higher than in BB&ECC and BB states. The unbalance of the current in the triple-fault state is much higher than in healthy one, slightly higher than in SHC&BB, higher than ECC&SHC and SHC states, Table 5.6.

Table 5.6 Information about the three phase currents in SHC&BB&ECC,

State	I_U [A]	I_V [A]	I_W [A]	I_m [A]	Current unbalance [%]
SHC&BB&ECC	8.9110	9.1557	8.7859	8.9509	2.2884

Table 5.7 Currents and Power through/in U1 and R_{SHC}, SHC&BB&ECC, SHC&BB, ECC&SHC and SHC states, load motor operation

State	I_{U1} [A]	P_{U1} [W]	I_{RSHC} [A]	P_{RSHC} [W]
SHC&BB&ECC	9.1602	16.153	5.3932	261.78

In SHC&BB&ECC state the value of the I_{U1} current is 9.1602 A, slightly higher than that in SHC&BB state and lower than the values in ECC&SHC and SHC states, Table 5.15.

The I_{U1} current is higher than the I_U current in SHC&BB&ECC and SHC&BB state, lower than I_U current in ECC&SHC and SHC states, Tables 5.6 and 5.7.

The power in the R_{SHC} resistor is 261.78 W, slightly lower than that in SHC&BB, ECC&SHC and SHC state. The power in R_{SHC} resistor is higher than in the U1 coil in each state that presents the SHC fault, Table 5.15.

5.3.1. Detection of triple-fault state through harmonics of I_U current

The first three harmonics of the I_U current with the highest values of the efficiency in SHC&BB&ECC detection are identical and in the same order like those in BB and SHC&BB states, consequently for the SHC&BB&ECC state can only be identified the BB fault and is not sure if here are other faults, Tables 5.16 and 5.17.

If the ECC fault occurs after the SHC&BB double-fault, the first three harmonics in the triple-fault will rest the same as in the SHC&BB state, consequently the triple fault cannot be differentiated from the double fault.

Also, if the SHC fault occurs after the BB&ECC double-fault only the third harmonic in the triple-fault will be different from those in the double-fault, consequently the triple fault can be differentiated from the double-fault.

But if the BB fault is superposed on the SHC&ECC fault, the first harmonic in the double-fault will be the third harmonic for the triple-fault and the first and second are the ones from BB state, consequently the triple-fault can be differentiated from the double-fault.

5.3.2. Detection of triple-fault state through harmonics of I_V current

The first three harmonics of the I_V current with the highest values of the efficiency in SHC&BB&ECC detection, 75 Hz, 100 Hz and 275 Hz, are identical and in the same order as those in SHC&BB and BB&ECC states, but the value of efficiency for 100 Hz harmonics is 42.7 % higher if the ECC fault is superposed on the SHC&BB double-fault and 86.39 % higher if the SHC fault is superposed on the BB&ECC double-fault, consequently if the value of efficiency in the fault detection corresponding to the 100 Hz harmonic is monitored the triple fault can be differentiated from the SHC&BB and BB&ECC double-fault states.

Also, the triple- fault harmonics are different from those in ECC&SHC, 150 Hz, 10 Hz and 1500 Hz, consequently the triple fault can be identified if a BB fault is superposed on the ECC&SHC double-fault.

Also, the triple-fault can be differentiated from the one-faults.

5.3.3. Detection of triple-fault state through harmonics of I_W current

For SHC&BB&ECC state, the first three harmonics with the highest values of efficiency in fault detection are the identical and in the same order with BB, SHC&BB and BB&ECC, consequently the triple- fault cannot be differentiated from those fault states.

The triple-fault can be differentiated from the SHC, ECC and ECC&SHC state if the first three harmonics are monitored during the life cycle of the induction motor.

CHAPTER 6 DETECTION OF FAULTS THROUGH MAGNETIC FLUX DENSITY IN THE MOTOR NEIGHBOURING

This chapter presents results related to the influence and diagnosis of the individual faults and their combination on the magnetic flux density, its components, in lateral part and proximity of the end windings, in order to identify the harmonics that characterize each fault for detection and identification in load motor operation(2880 rpm).

6.1. Detection of the one-faults

Points in the air region outside the motor, M[116, 0, 0] and N[-116, 0, 0], Figure 6.1., which are placed in the transversal symmetry plane z = 0 of the motor and P[116, 0, 90] and Q[-116, 0, 90], Fig. 6.1, in the plane z = 90 mm crossing the stator winding volume outside the magnetic core are considered for the evaluation of the radial component Bx and of the axial component Bz of the magnetic flux density.

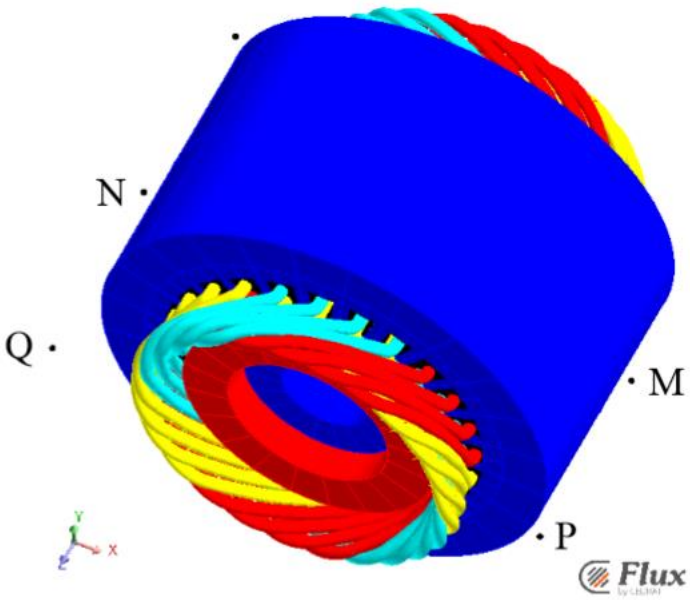

Fig. 6.1. Position of points for magnetic field evaluation

The impose criteria for harmonics to be taken into account is that efficiency in fault detection, equation 6.1 to be higher that 10 %.

Through harmonics of Bx[M]-Bx[N]

Fig. 6.2 presents the time variation of Bx[M]-Bx[N] for SHC, BB, ECC faults and HE state, LF analysis and in Fig. 6.3 from HF analysis.

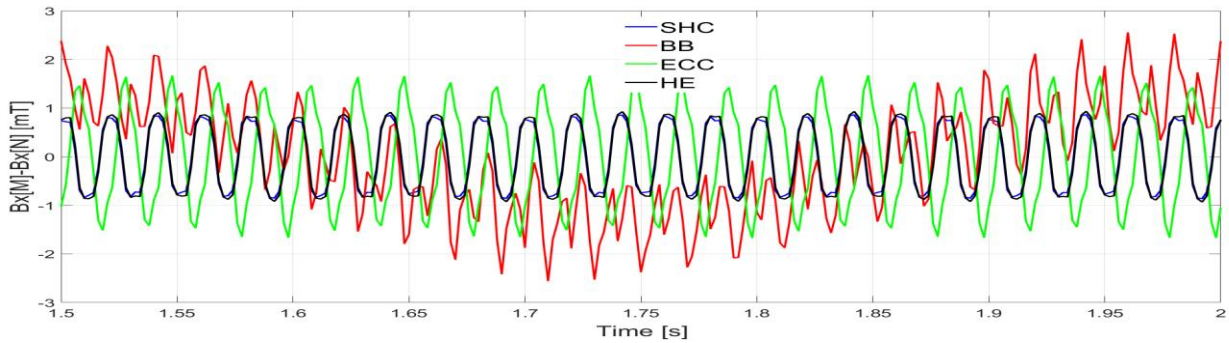

Fig. 6.2. Time variation of Bx[M]-Bx[N] for SHC, BB, ECC faults and HE state, LF analysis

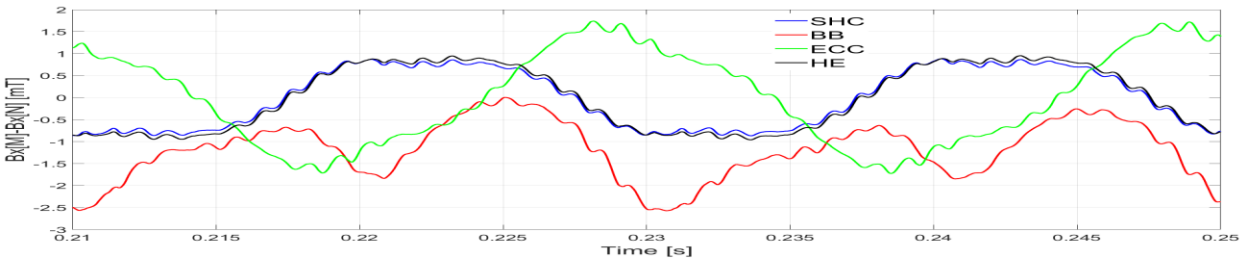

Fig. 6.3. Time variation of Bx[M]-Bx[N] for SHC, BB, ECC faults and HE state, HF analysis

The amplitudes of Bx[M]-Bx[N] harmonics for SHC, BB, ECC faults and HE state, LF analysis are presented in Fig. 6.4, in Figs. 6.4. and 6.5. for harmonics in the ranges [75 - 975] Hz and [1000 - 2000] Hz.

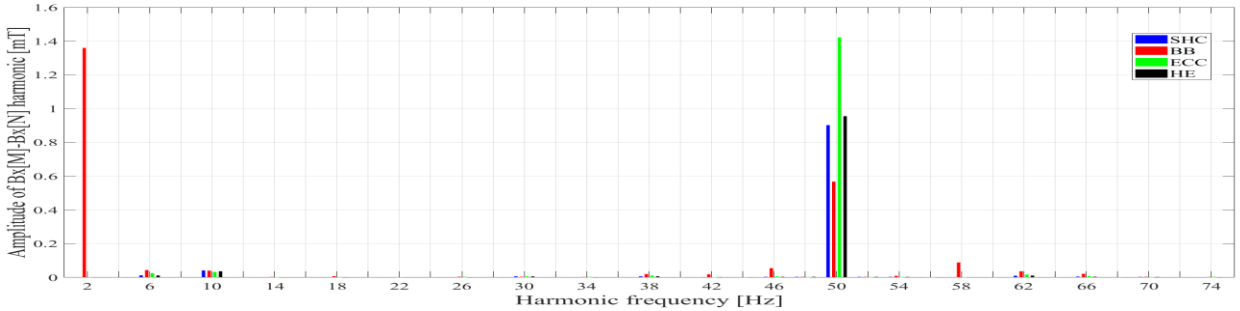

Fig. 6.4. Amplitudes of Bx[M]-Bx[N] harmonics for SHC, BB, ECC faults and HE state, LF analysis

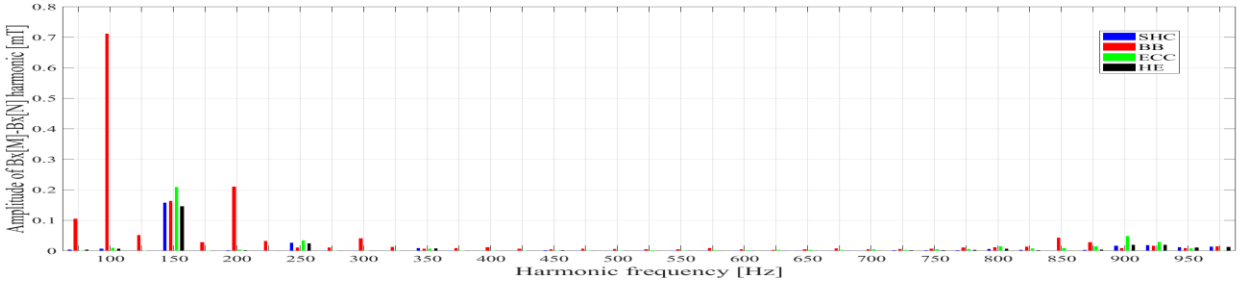

Fig. 6.5. Amplitudes of Bx[M]-Bx[N] harmonics in the range [75 - 975] Hz for SHC, BB, ECC faults and HE state, HF analysis

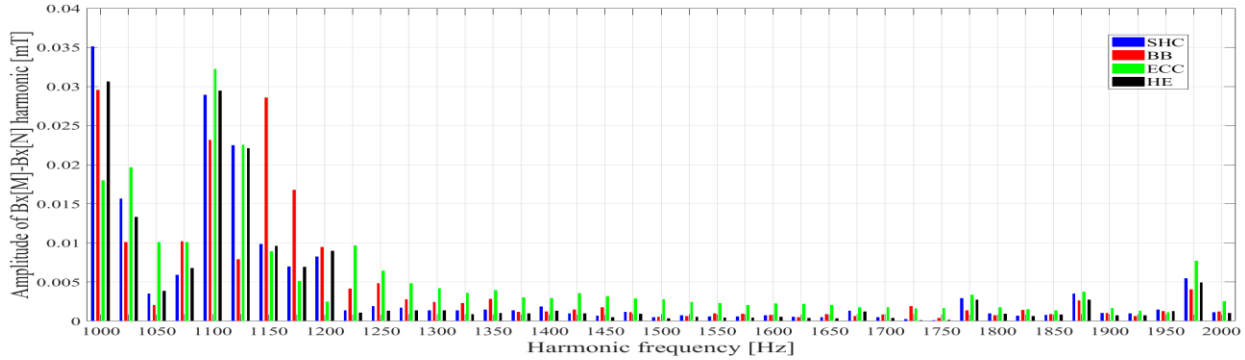

Fig. 6.6. Amplitudes of Bx[M]-Bx[N] harmonics in the range [1000 - 2000] Hz for SHC, BB, ECC faults and HE state, HF analysis

Through harmonics of Bz[P] + Bz[Q]

Fig. 6.7 presents the time variation of Bz[M]-Bz[N] for SHC, BB, ECC faults and HE state, LF analysis and in Fig. 6.8 from HF analysis.

The amplitudes of Bz[M]-Bz[N] harmonics for SHC, BB, ECC faults and HE state, LF analysis are presented in Fig. 6.9, in Figs. 6.10. and 6.11. for harmonics in the ranges [75 - 975] Hz and [1000 - 2000] Hz.

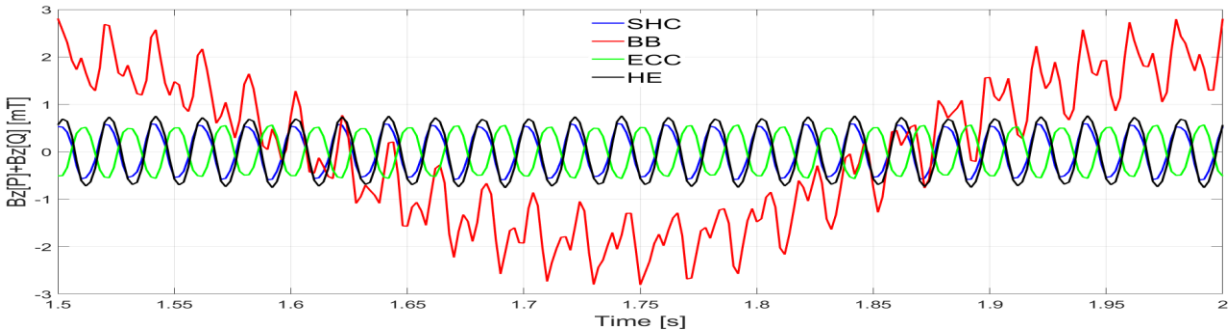

Fig. 6.7. Time variation of Bz[P]+Bz[Q] for SHC, BB, ECC faults and HE state, LF analysis

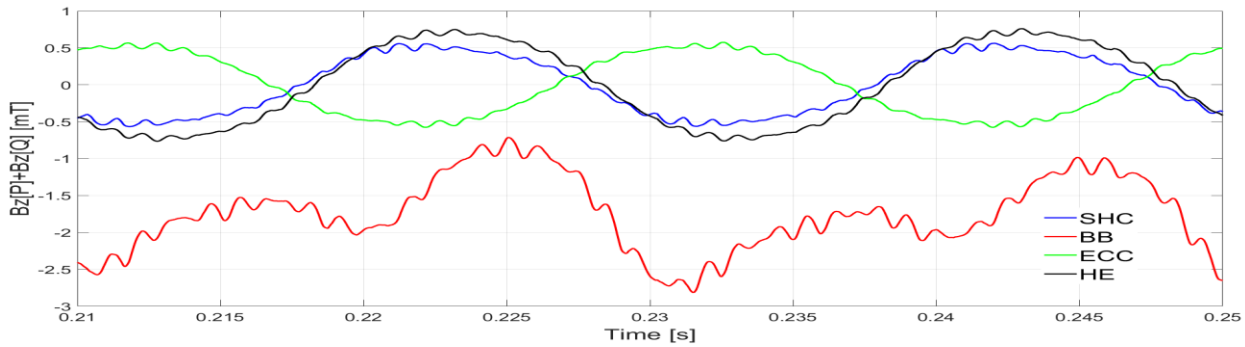

Fig. 6.8. Time variation of Bz[P]+Bz[Q] for SHC, BB, ECC faults and HE state, LF analysis

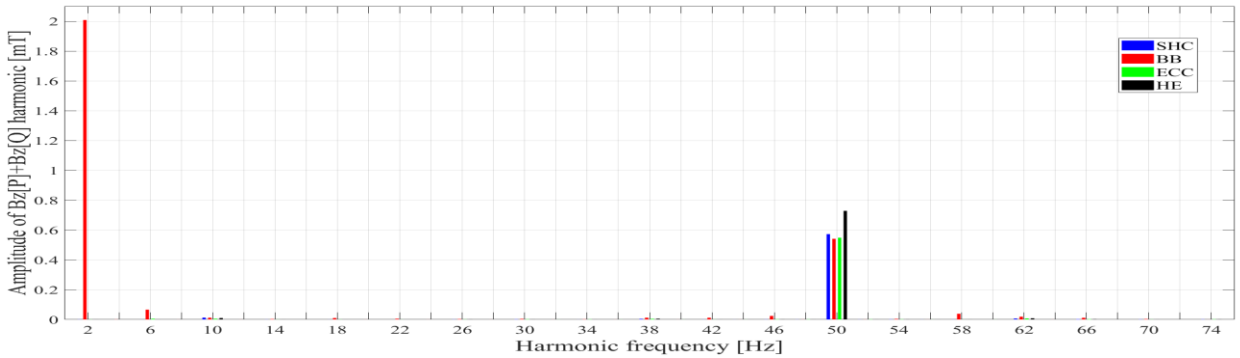

Fig. 6.9. Amplitudes of Bz[P]+Bz[Q] harmonics for SHC, BB, ECC faults and HE state, LF analysis

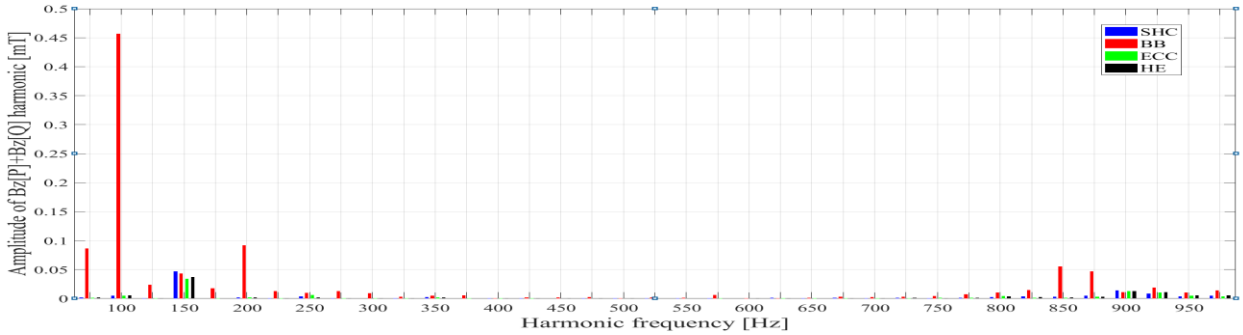

Fig. 6.10. Amplitudes of Bz[P]+Bz[Q] harmonics in the range [75 - 975] Hz for SHC, BB, ECC faults and HE state, HF analysis

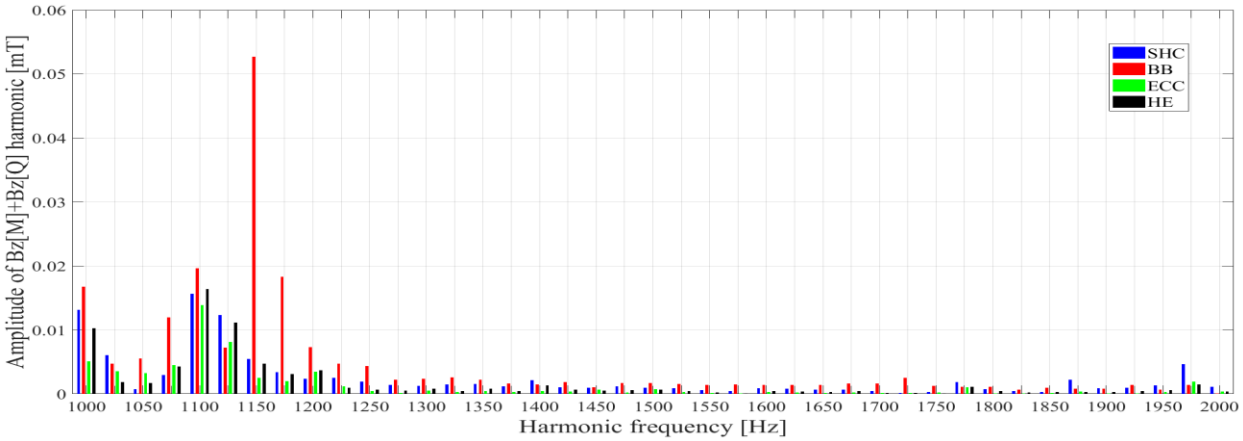

Fig. 6.11. Amplitudes of Bz[P]+Bz[Q] harmonics in the range [1000 - 2000] Hz for SHC, BB, ECC faults and HE state, HF analysis

Table 6.1 presents the highest values of the efficiency in fault detection for SHC, BB and ECC one-faults.

Table 6.1 The highest values of efficiency in one-faults detection

	SHC	**BB**	**ECC**
Efficiency	3.256	2364	18.59
f [Hz]	1025	2	6
Component	Bz(P)+Bz[Q]	Bz(P)+Bz[Q]	Bz(P)+Bz[Q]

Concerning the SHC fault, the most sensitive magnetic flux density harmonics are: the 1025 Hz of Bz[P] + Bz[Q] with an amplitude increase of 3.256 times, 800 Hz of By[P]-By[Q] with 3.085 increase and 1975 Hz of Bx[P]-Bx[Q] with 2.631 increase. Those are harmonics of the magnetic field near the end windings.

Regarding the BB fault, the 2 Hz harmonic of Bz[P] + Bz[Q] has the highest amplitude increase of 2364 times, followed by the 2 Hz harmonic of Bx[M]-Bx[N] with 1386 increase and 2 Hz harmonic of By[P]-By[Q] with 366.5 increase.

The ECC fault can be detected through the 6 Hz harmonic of Bz[P] + Bz[Q], that has an amplitude increase of 18.59 times or 825 Hz harmonic of Bx[M] characterized by an increase of 17.02 times or 1100 Hz of By[P]-By[Q] with an increase of 14.43 times.

Was found that through the harmonics of Bz[P] + Bz[Q], the three fault can be detected and differentiated, because the most influenced harmonic by a certain fault is different, 1025 Hz for SHC, 2 Hz for BB and 6 Hz for ECC.

6.2. Detection of the double faults

The highest values of efficiency in double fault detection are presented is Table 6.2.

Table 6.2 The highest values of efficiency in double fault detection

	SHC&BB	**BB&ECC**	**ECC&SHC**
Efficiency	2363	1941	23.53
f [Hz]	2	2	6
Component	Bz[P] + Bz[Q]	Bz[P] + Bz[Q]	Bz[P] + Bz[Q]

In the case of SHC&BB fault, the most sensible harmonics are: 2 Hz harmonic of Bz[P] + Bz[Q] that has an amplitude increase of 2363 times, 2 Hz harmonics of Bx[M]-Bx[N], with an efficiency of 1386 times, and 2 Hz harmonics of By[P]-By[Q], that has an 367.9 efficiency.

Concerning the BB&ECC fault, 2 Hz harmonic of Bz[P] + Bz[Q] has the highest value of efficiency of 1941, the next ones are 2 Hz harmonics of Bx[M]-Bx[N], with an efficiency of 1431 and 2 Hz harmonics of Bx[P]-Bx[Q], with an efficiency of 445.8.

For SHC&ECC faults was found that 6 Hz harmonic of Bz[P] + Bz[Q] has the highest value of efficiency, 23.53, the next two ones are 825 Hz harmonic of Bx[M] with 16.37 efficiency, and 850 Hz harmonic of Bx[M]-Bx[N] with a efficiency of 16.26.

Regarding the triple fault SHC&BB&ECC, this fault has the most influence on 2 Hz harmonic of Bz[P] + Bz[Q], with an increase of 1938 times, 2 Hz harmonic of Bx[M]-Bx[N], that has an increase of 1429 times, and 2 Hz harmonic of Bx[P]-Bx[Q], with 449.8 times increase.

In case of SHC&BB fault, the 100 Hz harmonic of By[M] if the first one, with a efficiency of 48.47, for the BB&ECC the first harmonic is the 200 Hz, with a efficiency of 73.26 and in case of ECC&SHC is the 1100 Hz harmonic, with a efficiency of 2.749. Therefore, the double faults can be detected and differentiated through the harmonics of the By[M].

Through the harmonics of the By[P]-By[Q], the double faults can be detected and differentiated because for the SHC&BB fault the harmonicas with the highest efficiency of 367.9 is the 2 Hz one, for BB&ECC is the 46 Hz one, but has similar value of efficiency as the 2 Hz one., with 232.5 efficiency and 1100 Hz, with a efficiency of 14.54 for ECC&SHC.

6.3. Detection of the triple fault, SHC&BB&ECC

Table 6.3. presents the efficiency in SHC&BB&ECC fault detection through LF&HF harmonics of Bz[P] + Bz[Q]. It can be seen that the 2 Hz harmonic has the highest efficiency.

Table 6.3 Efficiency in SHC&BB&ECC fault detection through LF&HF harmonics of Bz[P] + Bz[Q]

f [Hz]	2	6	58	100	300	22	175	200	18	75
SHC&BB&ECC [μT]	1645	54.43	35.66	362	25.42	5.205	11.71	76.34	8.123	71.27
HE [μT]	0.849	0.253	0.486	5.327	0.411	0.0934	0.223	1.818	0.211	1.934
SHC&BB&ECC/HE	1938	215	73.43	67.96	61.9	55.74	52.63	42	38.54	36.84

CHAPTER 7 EXPERIMENTAL INVESTIGATION OF SHORT-CIRCUIT FAULT

In this chapter are presented the experimental and finite element results obtained from the analysis of the influence of short-circuit fault on the magnetic field in the vicinity of induction motors investigated through the time variation of the output voltage of coil sensors in case of healthy and faulty motor states, for no load/loaded motor operation.

7.1. Experimental results obtained for the induction motor under short-circuit fault

In this subsection are presented the experimental results for the two poles induction motor for no-load operation in three positions for the coil sensors:

Fig. 7.1. Experimental system for external magnetic field investigation and artificial short-circuits generation

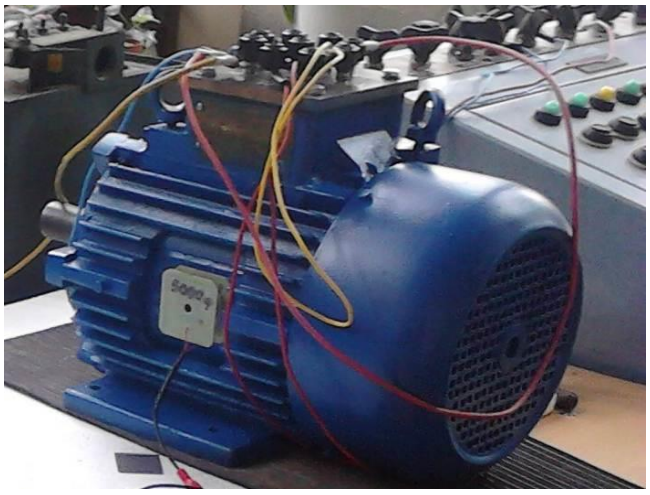

Fig. 7.2. Coil Sensor_Ox2 position near the stator core

Experimental results when the coil Sensor_Ox2 is in the position from Figure 7.2 and coil Sensor_Ox1 is at 180 degrees from the other coil sensor

The results are obtained for three cases: healthy HE0, weak fault when the current through the variable resistor is 5 A, FA05, and strong fault when the current is 10 A, FA10.

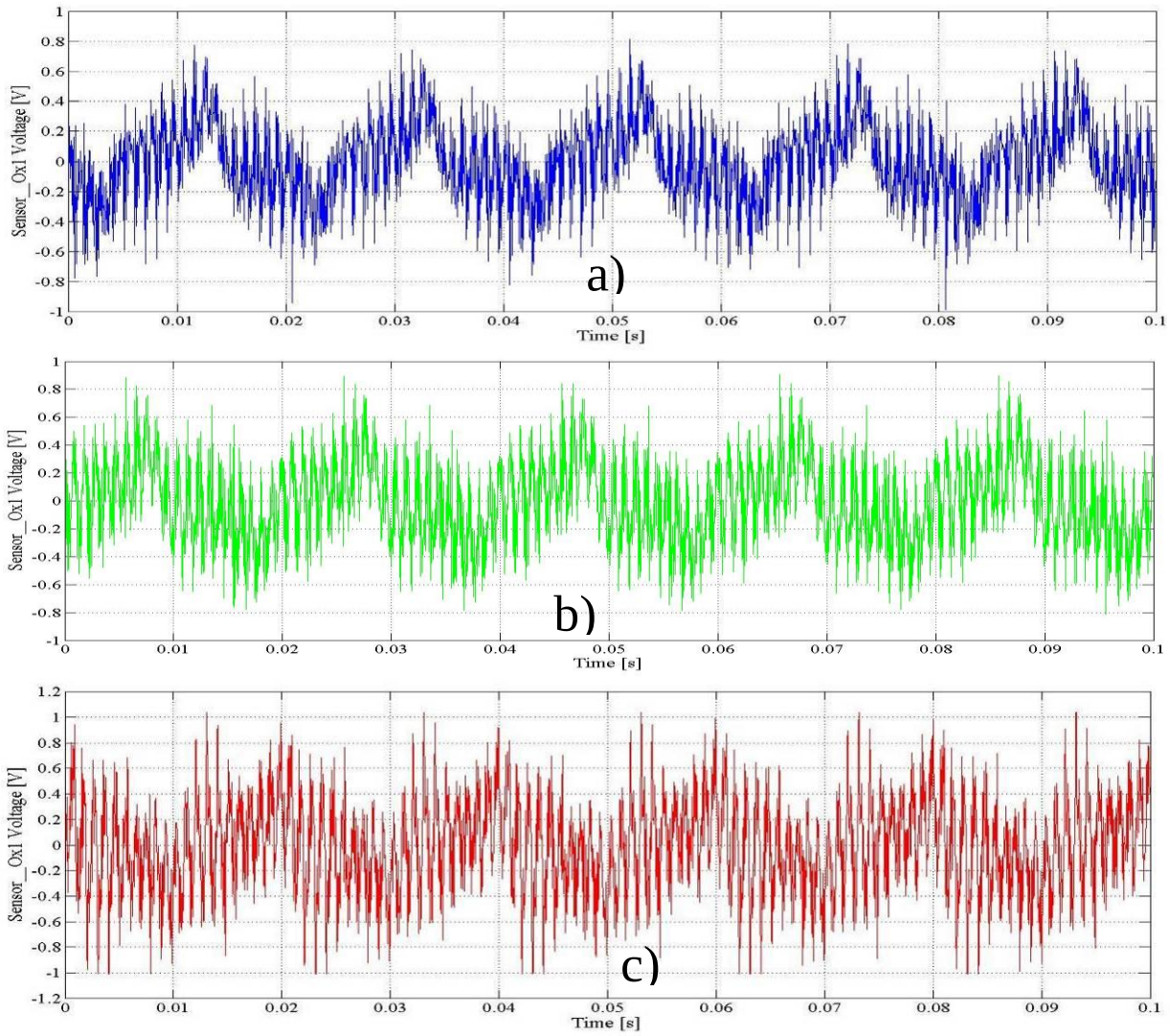

Fig. 7.3. Time variation of Sensor_Ox1 Voltage for a) healthy, b) weak fault and c) strong fault cases

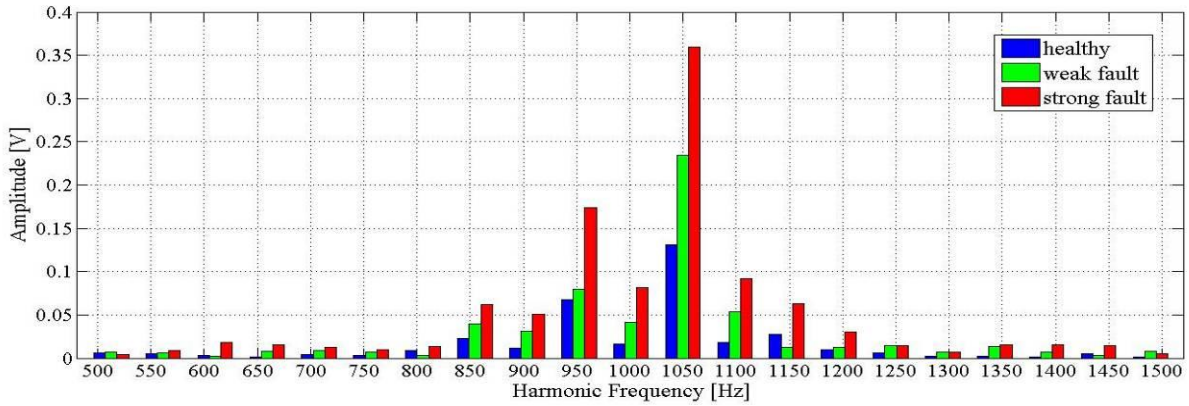

Fig. 7.4. Amplitude of harmonics of Sensor_Ox1 voltage

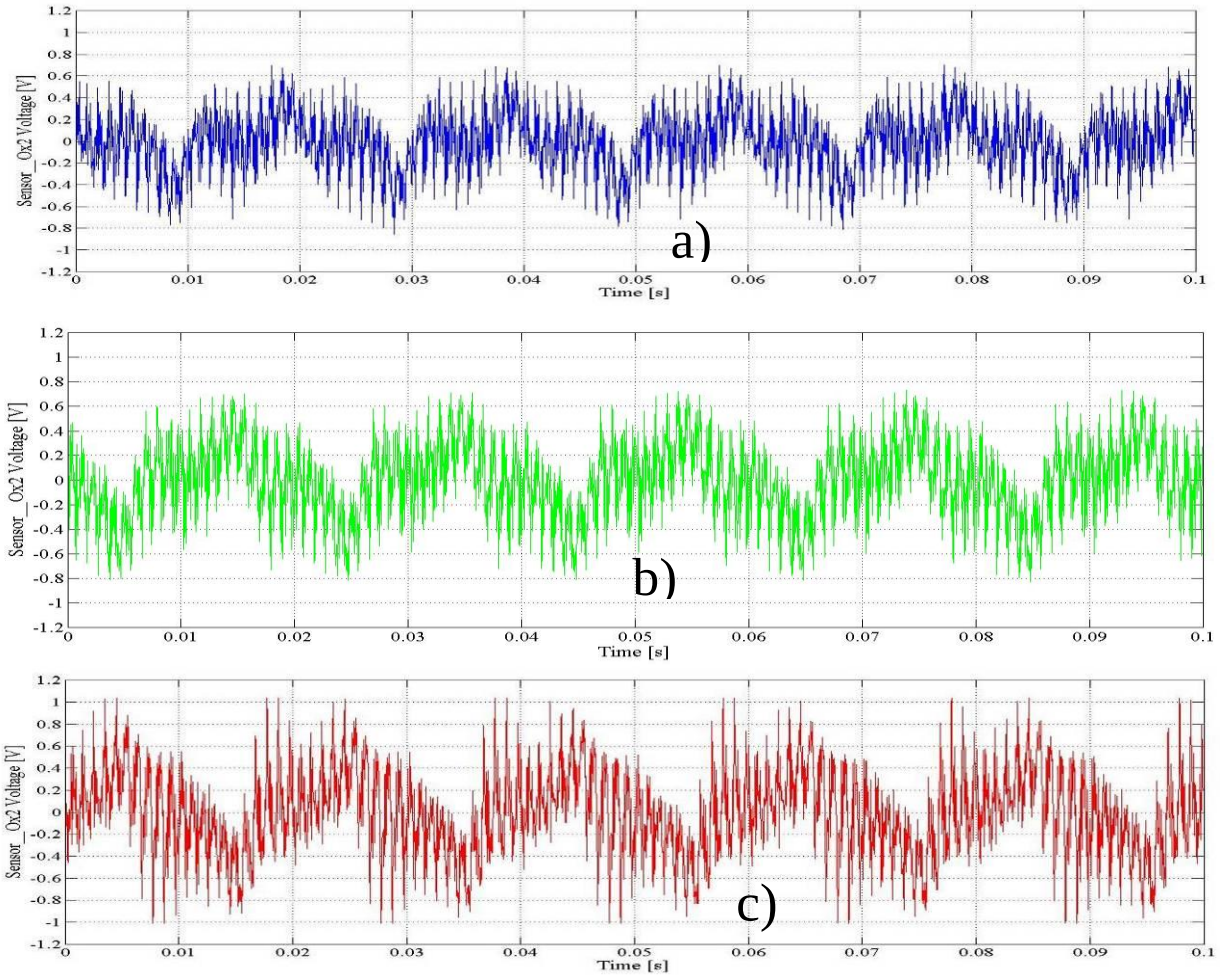

Fig. 7.5. Time variation of Sensor_Ox2 Voltage for a) healthy, b) weak fault and c) strong fault cases

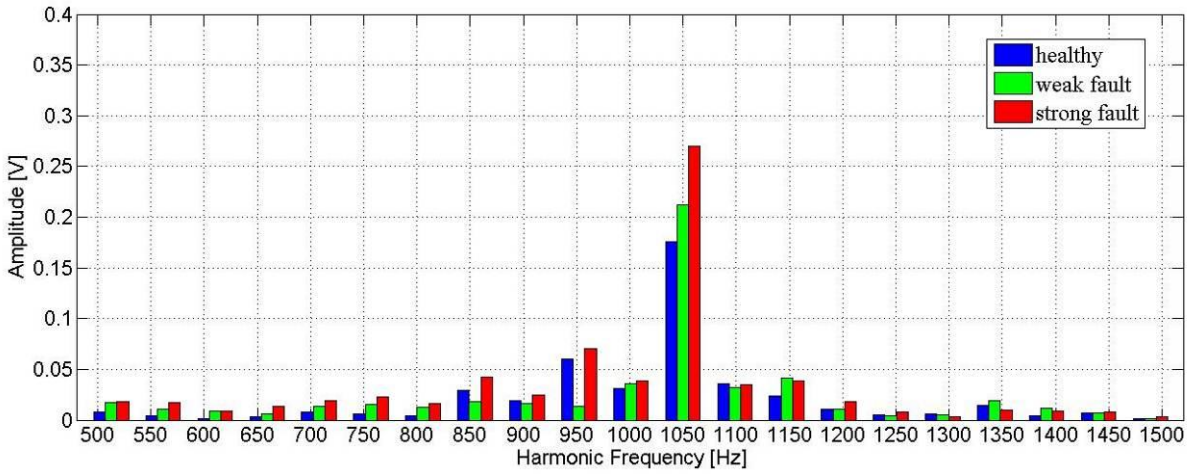

Fig. 7.6. Amplitude of harmonics of Sensor_Ox2 voltage

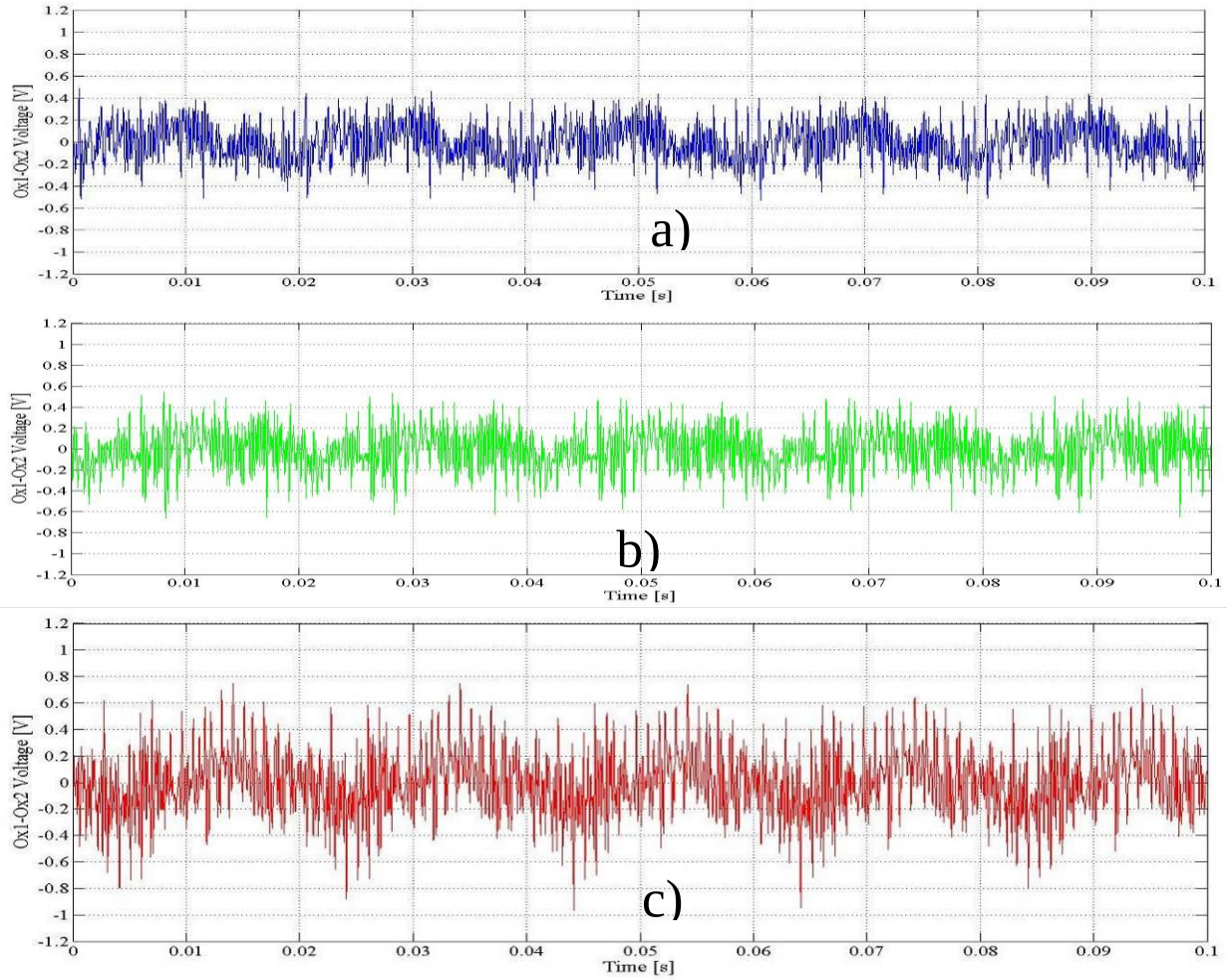

Fig. 7.7. Time variation of Ox1-Ox2 Voltage for a) healthy, b) weak fault and c) strong fault cases

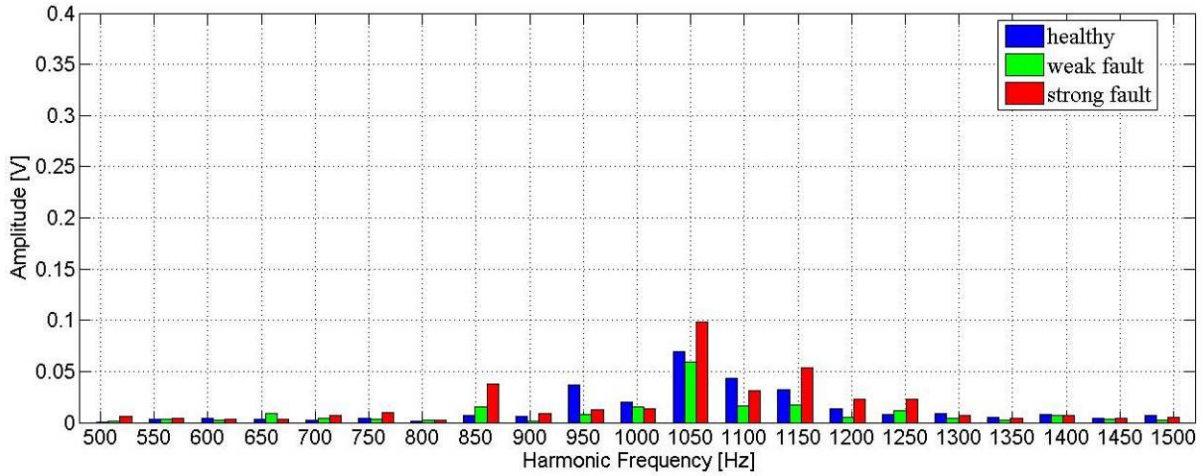

Fig. 7.8. Amplitude of harmonics of Ox1-Ox2 voltage

The rms values of the Ox1, Ox2 and Ox1-Ox2 voltages for healthy, HE0, and faulty induction motor, FA05 and FA10 are presented in Table 7.1. The values are higher when the induction motor is faulty.

Table 7.1. Rms values for coil sensors output voltages [V]

	SensorOx1	SensorOx2	Ox1-Ox2
HE0	0.279	0.287	0.179
FA01	0.315	0.321	0.197
FA02	0.390	0.394	0.245

GENERAL CONCLUSIONS, THESIS CONTRIBUTIONS AND PROPORSALS FOR FUTURE RESEARCHES

C1. GENERAL CONCLUSIONS

The faults have influence on the mean value of the electromagnetic torque of the induction motor and creates a rotor unbalanced force, due to a non-symmetry of the magnetic field inside the induction motor, force that will act on the bearings shortening their lifespan. The force is also present in load and no-load operation.

Through the harmonics of the phase currents can be detected if a fault is SHC, BB or ECC.

The double-faults states can be detected through the harmonics of the phase currents if the first three harmonics and their efficiency in one-faults detection are known.

The triple-fault can be differentiated from the SHC, ECC and ECC&SHC state if the first three harmonics are monitored during the life cycle of the induction motor.

The first three harmonics of the I_U current with the highest values of the efficiency in SHC&BB&ECC detection are identical and in the same order like those in BB and SHC&BB states, consequently for the SHC&BB&ECC state can only be identified the BB fault and is not sure if here are other faults. If the ECC fault occurs after the SHC&BB double-fault, the first three harmonics in the triple-fault will rest the same as in the SHC&BB state, consequently the triple fault cannot be differentiated from the double fault. Also, if the SHC fault occurs after the BB&ECC double-fault only the third harmonic in the triple-fault will be different from those in the double-fault, consequently the triple fault can be differentiated from the double-fault. But if the BB fault is superposed on the SHC&ECC fault, the first harmonic in the double-fault will be the third harmonic for the triple-fault and the first and second are the ones from BB state, consequently the triple-fault can be differentiated from the double-fault.

The first three harmonics of the I_V current with the highest values of the efficiency in SHC&BB&ECC detection, 75 Hz, 100 Hz and 275 Hz, are identical and in the same order as those in SHC&BB and BB&ECC states, but the value of efficiency for 100 Hz harmonics is 42.7 % higher if the ECC fault is superposed on the SHC&BB double-fault and 86.39 % higher if the SHC fault is superposed on the BB&ECC double-fault, consequently if the value of efficiency in the fault detection corresponding to the 100 Hz harmonic is monitored the triple fault can be differentiated from the SHC&BB and BB&ECC double-fault states. Also, the triple- fault harmonics are different from those in ECC&SHC, 150 Hz, 10 Hz and 1500 Hz, consequently the triple fault can be identified if a BB fault is superposed on the ECC&SHC double-fault.Also, the triple-fault can be differentiated from the one-faults.

For SHC&BB&ECC state, the first three harmonics with the highest values of efficiency in fault detection are the identical and in the same order with BB, SHC&BB and BB&ECC, consequently the triple- fault cannot be differentiated from those fault states. The triple-fault can be differentiated from the SHC, ECC and ECC&SHC state if the first three harmonics are monitored during the life cycle of the induction motor.

Through the magnetic field outside the motors especially near the ends of the windings, the mono-faults and the double-faults scan be detected and differentiated, for the triple fault is a little bit complicated, because is important to know the evolution of the fault in order to differentiate it than the other ones.

From the experimental results it was seen that the short-circuit fault can be detected through the rms values or the altitudes of the harmonics of the voltages induced in the field coils or the substitution of those voltages.

C2. THESIS CONTRIBUTIONS

The original contribution consists firstly in developing the 3D finite element models using commercial software Altair Flux 3D for study of three types of different faults short-circuit, broken bar, static eccentricity and their combinations.

The time domain studies were performed for healthy state, one-faults, double-faults (short-circuit and broken bar and static eccentricity, static eccentricity and short-circuit), and triple-fault(short-circuit and broken bar and static eccentricity). Two 3D finite element models for each case were developed in order to analyses low harmonics in the range [2 Hz; 74 Hz] and high harmonics in range [75 Hz; 200 Hz]. Each 3D model take 3 weeks to solve and results around 300 GB of data.

The definition of Efficiency in fault detection value of harmonic amplitude in faulty state)/(value of harmonic amplitude in healthy state)=FA/HE.

In order the compute the efficiency in fault detection, FFT analysis were performed for phase currents and the components of the magnetic flux density in the symmetry plane and in the vicinity of the ends of the windings.

C3. PROPORSAL FOR FUTURE PERSPECTIVES

As future perspective I would like to obtain some experimental results concerning the, mono, double and, the triple fault, currents, voltages induced in the field coils, torque to measure the rotor unbalanced force and compare the results obtained data with the simulations.

REFERENCES

[1] Nandi, S.; Toliyat, H.A.; Li, X. Condition Monitoring and Fault Diagnosis of Electrical Motors—A Review. IEEE Trans. Energy Convers. 2005, 20, 719–729.

[2] Thorsen, O.V.; Dalva, M. Failure Identification and Analysis for High-Voltage Induction Motors in the Petrochemical Industry. IEEE Trans. Ind. Appl. 1999, 35, 810–818.

[3] Bell, R.N.; Heising, C.R.; O'Donnell, P.;Wells, S.J.; Singh, C. Report of Large Motor Reliability Survey of Industrial and Commercial Installations, Part II. IEEE Trans. Ind. Appl. 1985, IA-21, 865–872.

[4] Sa'ad Ahmed Saleh Al Kazzaz, G.K Singh, Experimental investigations on induction machine condition monitoring and fault diagnosis using digital signal processing techniques, Electric Power Systems Research, Volume 65, Issue 3, 2003, Pages 197-221, ISSN 0378-7796, https://doi.org/10.1016/S0378-7796(02)00227-4.

[5] M. R. W. Group, “Report of large motor reliability survey of industrial and commercial installations, part ii,” IEEE Transactions on Industry Applications, vol. IA-21, no. 4, pp. 865–872, July 1985.
[6] Asad, B.; Vaimann, T.; Rassõlkin, A.; Kallaste, A.; Belahcen, A. A Survey of Broken Rotor Bar Fault Diagnostic Methods of Induction Motor. Electr. Control. Commun. Eng. 2018, 14, 117–124.
[7] Bellini, A.; Filippetti, F.; Tassoni, C.; Capolino, G.-A. Advances in Diagnostic Techniques for Induction Machines. IEEE Trans. Ind. Electron. 2008, 55, 4109–4126.
[8] Alsaedi, M.A. Fault Diagnosis of Three-Phase Induction Motor: A Review. Optics 2015, 4, 1–8.
[9] Sardar, M.U.; Vaimann, T.; Kütt, L.; Kallaste, A.; Asad, B.; Akbar, S.; Kudelina, K. Inverter-Fed Motor Drive System: A Systematic Analysis of Condition Monitoring and Practical Diagnostic Techniques. Energies 2023, 16, 5628.
[10] Cho, D.H.; Jung, H.K.; Chung, T.K.; Lee, C.G. Design of a Short-Time Rating Interior Permanent Magnet Synchronous Motor Using a Niching Genetic Algorithm. IEEE Trans. Magn. 2000, 36, 1936–1940.
[11] Yun, J.; Park, S.; Yang, C.; Park, Y.; Lee, S.B.; Šaši´c, M.; Stone, G.C. Comprehensive Monitoring of Field Winding Short Circuits for Salient Pole Synchronous Motors. IEEE Trans. Energy Convers. 2019, 34, 1686–1694.
[12] Cherif, H.; Menacer, A.; Romary, R.; Pusca, R. Dispersion Field Analysis Using Discrete Wavelet Transform for Inter-Turn Stator Fault Detection in Induction Motors. In Proceedings of the 2017 IEEE 11th International Symposium on Diagnostics for Electrical Machines, Power Electronics and Drives, SDEMPED 2017, Tinos, Greece, 29 August–1 September 2017.
[13] Kim, T.H.; Lee, J. Comparison of the Iron Loss of a Flux-Reversal Machine under Four Different PWM Modes. IEEE Trans. Magn. 2007, 43, 1725–1728.
[14] de Souza, R.P.P.; Agulhari, C.M.; Goedtel, A.; Castoldi, M.F. Inter-Turn Short-Circuit Fault Diagnosis Using Robust Adaptive Parameter Estimation. Int. J. Electr. Power Energy Syst. 2022, 139, 107999.
[15] Das, S.; Purkait, P.; Dey, D.; Chakravorti, S. Monitoring of Inter-Turn Insulation Failure in Induction Motor Using Advanced Signal and Data Processing Tools. IEEE Trans. Dielectr. Electr. Insul. 2011, 18, 1599–1608.
[16] Liang, H.; Chen, Y.; Liang, S.;Wang, C. Fault Detection of Stator Inter-Turn Short-Circuit in Pmsm on Stator Current and Vibration Signal. Appl. Sci. 2018, 8, 1677. [CrossRef]
[17] Praveen Kumar, N.; Isha, T.B. FEM Based Electromagnetic Signature Analysis of Winding Inter-Turn Short-Circuit Fault in Inverter Fed Induction Motor. CES Trans. Electr. Mach. Syst. 2019, 3, 309–315.
[18] Hong, J.; Park, S.; Hyun, D.; Kang, T.J.; Lee, S.B.; Kral, C.; Haumer, A. Detection and Classification of Rotor Demagnetization and Eccentricity Faults for PM Synchronous Motors. IEEE Trans. Ind. Appl. 2012, 48, 923–932.
[19] Terron-Santiago, C.; Martinez-Roman, J.; Puche-Panadero, R.; Sapena-Bano, A. A Review of Techniques Used for Induction Machine Fault Modelling. Sensors 2021, 21, 4855.
[20] Edomwandekhoe, K.; Liang, X. Current Spectral Analysis of Broken Rotor Bar Faults for Induction Motors. In Proceedings of the Canadian Conference on Electrical and Computer Engineering, Quebec City, QC, Canada, 13–16 May 2018.
[21] Spyropoulos, D.V.; Gyftakis, K.N.; Kappatou, J.; Mitronikas, E.D. The Influence of the Broken Bar Fault on the Magnetic Field and Electromagnetic Torque in 3-Phase Induction Motors. In Proceedings of the 2012 20th International Conference on Electrical Machines, ICEM, Marseille, France, 2–5 September 2012.

[22] Goktas, T.; Arkan, M.; Salih Mamis, M.; Akin, B. Broken Rotor Bar Fault Monitoring Based on Fluxgate Sensor Measurement of Leakage Flux. In Proceedings of the 2017 IEEE International Electric Machines and Drives Conference, IEMDC, Miami, FL, USA,21–24 May 2017.

[23] Asad, B.; Eensalu, L.; Vaimann, T.; Kallaste, A.; Rassolkin, A.; Belahcen, A. The FEM Based Modeling and Corresponding Test Rig Preparation for Broken Rotor Bars Analysis. In Proceedings of the 2019 IEEE 60th Annual International Scientific Conference on Power and Electrical Engineering of Riga Technical University, RTUCON, Riga, Latvia, 7–9 October 2019.

[24] Constantin, A.I. Detection Based on Stator Current Signature of the Single and Combined Short-Circuit, Broken Bar and Eccentricity Faults in Induction Motors. In Proceedings of the 2019 11th International Symposium on Advanced Topics in Electrical Engineering, ATEE, Bucharest, Romania, 28–30 March 2019.

[25] Sobczyk, T.J.; Tulicki, J.; Weinreb, K.; Mielnik, R.; Sulowicz, M. Characteristic Features of Rotor Bar Current Frequency Spectrum in Cage Induction Machine with Inner Faults. In Proceedings of the 2019 IEEE 12th International Symposium on Diagnostics for Electrical Machines, Power Electronics and Drives, SDEMPED, Toulouse, France, 27–30 August 2019.

[26] Jannati, M.; Idris, N.R.N.; Salam, Z. A New Method for Modeling and Vector Control of Unbalanced Induction Motors. In Proceedings of the 2012 IEEE Energy Conversion Congress and Exposition, ECCE, Raleigh, NC, USA, 15–20 September 2012.

[27] Malekpour, M.; Phung, B.T.; Ambikairajah, E. Online Technique for Insulation Assessment of Induction Motor Stator Windings under Different Load Conditions. IEEE Trans. Dielectr. Electr. Insul. 2017, 24, 349–358.

[28] Zoeller, C.; Vogelsberger, M.A.; Wolbank, T.M.; Ertl, H. Impact of SiC Semiconductors Switching Transition Speed on Insulation Health State Monitoring of Traction Machines. IET Power Electron. 2016, 9, 2769–2775.

[29] Cavallini, A.; Montanari, G.C.; Fabiani, D.; Tozzi, M. The Influence of PWM Voltage Waveforms on Induction Motor Insulation Systems: Perspectives for the End User. In Proceedings of the SDEMPED 2011—8th IEEE Symposium on Diagnostics for Electrical Machines, Power Electronics and Drives, Bologna, Italy, 5–8 September 2011.

[30] Faiz, J.; Ojaghi, M. Unified Winding Function Approach for Dynamic Simulation of Different Kinds of Eccentricity Faults in Cage Induction Machines. IET Electr. Power Appl. 2009, 3, 461–470.

[31] TOUHAMI, O.; AIBECHE, A.; ABDELLI, R.; BOUZIDA, A. Dynamic Eccentricity Fault Diagnosis in Induction Motors Using Finite Element Method and Experimental Tests. Int. J. Ind. Electron. Drives 2017, 3, 199–209.

[32] Sobra, J.; Vaimann, T.; Belahcen, A. Mechanical Vibration Analysis of Induction Machine under Dynamic Rotor Eccentricity. In Proceedings of the Proceedings—2016 17th International Scientific Conference on Electric Power Engineering, EPE 2016, Prague,Czech Republic, 16–18 May 2016.

[33] Alfredo Munoz, R.; Gonzalo Nahmias, C. Mechanical Vibration of Three-Phase Induction Motors Fed by Nonsinusoidal Currents. In Proceedings of the 3rd International Power Electronics Congress—CIEP, Puebla, Mexico, 21–25 August 1994.

[34] Luo, G.; Habetler, T.G.; Hurwitz, J. Stray Flux-Based Incipient Stage Bearing Fault Detection for Induction Machines via Noise Cancellation Techniques. In Proceedings of the ECCE 2020—IEEE Energy Conversion Congress and Exposition, Detroit, MI, USA, 11–15 October 2020.

[35] Fireteanu, V.; Lombard, P.; Constantin, A.I. Detection of a Short-Circuit Fault in the Stator Winding of Induction Motors through Neighboring Magnetic Field Harmonics. In Proceedings of the 2014

International Conference on Electrical Machines, ICEM 2014, Berlin, Germany, 2–5 September 2014.

[36] Frosini, L.; Harlisca, C.; Szabo, L. Induction Machine Bearing Fault Detection by Means of Statistical Processing of the Stray Flux Measurement. IEEE Trans. Ind. Electron. 2015, 62, 1846–1854.

[37] Yea, M.; Han, K.J. Modified Slot Opening for Reducing Shaft-to-Frame Voltage of AC Motors. Energies 2020, 13, 760.

[38] Lopes, P.J.A.; Soares, F.J.; Almeida, R.P.M.; Baptista, P.C.; Silva, C.M.; Farias, T.L. Quantification of Technical Impacts and Environmental Benefits of Electric Vehicles Integration on Electricity Grids. In Proceedings of the 2009 8th International Symposium on Advanced Electromechanical Motion Systems and Electric Drives Joint Symposium, ELECTROMOTION, Lille, France, 1–3 July 2009.

[39] Balaram, V. Rare Earth Elements: A Review of Applications, Occurrence, Exploration, Analysis, Recycling, and Environmental Impact. Geosci. Front. 2019, 10, 1285–1303.

[40] Zaripova, A.D.; Zaripov, D.K.; Usachev, A.E. Visualization of High-Voltage Insulators Defects on Infrared Images Using Computer Vision Methods. Sci. Vis. 2019, 11, 88–98. [CrossRef]

[41] Plazenet, T.; Boileau, T.; Caironi, C.; Nahid-Mobarakeh, B. An Overview of Shaft Voltages and Bearing Currents in Rotating Machines. In Proceedings of the IEEE Industry Application Society, 52nd Annual Meeting: IAS 2016, Portland, OR, USA, 2–6 October 2016.

[42] Alger, P.L.; Samson, H.W. Shaft Currents in Electric Machines. Trans. Am. Inst. Electr. Eng. 1924, 43, 235–245.

[43] Kerszenbaum, I. Shaft Currents in Electric Machines Fed by Solid-State Drives. In Proceedings of the IEEE Conference Record of Industrial and Commercial Power Systems Technical Conference, Pittsburgh, PA, USA, 4–7 May 1992.

[44] Mocanu, R.; Onea, A. Determination of Stator Temperature for Thermal Protection in a Permanent Magnet Synchronous Machine. In Proceedings of the 2017 25th Mediterranean Conference on Control and Automation, MED, Valletta, Malta, 3–6 July 2017.

[45] Nair, D.G.; Rasilo, P.; Arkkio, A. Sensitivity Analysis of Inverse Thermal Modeling to Determine Power Losses in Electrical Machines. IEEE Trans. Magn. 2018, 54, 8109405.

[46] Wallscheid, O.; Böcker, J. Global Identification of a Low-Order Lumped-Parameter Thermal Network for Permanent Magnet Synchronous Motors. IEEE Trans. Energy Convers. 2016, 31, 354–365.

[47] Choudhary, A.; Goyal, D.; Shimi, S.L.; Akula, A. Condition Monitoring and Fault Diagnosis of Induction Motors: A Review. Arch. Comput. Methods Eng. 2019, 26, 1221–1238.

[48] Tita, M.C.; Bitoleanu, A. Technologies and Pollution Factors in Electrical Machines Factory. In Proceedings of the 2012 International Conference on Applied and Theoretical Electricity, ICATE, Craiova, Romania, 25–27 October 2012.

[49] Lopez-Perez, D.; Antonino-Daviu, J. Application of Infrared Thermography to Failure Detection in Industrial Induction Motors: Case Stories. IEEE Trans. Ind. Appl. 2017, 53, 1901–1908.

[50] Sheikh, M.A.; Nor, N.M.; Ibrahim, T.; Bin Hamdan, M.F. A New Method for Detection of Unbalanced Voltage Supply through Rotor Harmonics and Symbolic State Dynamics. In Proceedings of the International Conference on Intelligent and Advanced Systems, ICIAS 2016, Kuala Lumpur, Malaysia, 15–17 August 2016.

[51] Jlassi, I.; Estima, J.O.; El Khil, S.K.; Bellaaj, N.M.; Cardoso, A.J.M. A Robust Observer-Based Method for IGBTs and Current Sensors Fault Diagnosis in Voltage-Source Inverters of PMSM Drives. IEEE Trans. Ind. Appl. 2017, 53, 2894–2905.

[52] Bourogaoui, M.; Sethom, H.B.A.; Belkhodja, I.S. Speed/Position Sensor Fault Tolerant Control in Adjustable Speed Drives—A Review. ISA Trans. 2016, 64, 269–284.
[53] Quang, N.K.; Hieu, N.T.; Ha, Q.P. FPGA-Based Sensorless PMSM Speed Control Using Reduced-Order Extended Kalman Filters. IEEE Trans. Ind. Electron. 2014, 61, 6574–6582.
[54] Chen, C.X.; Xie, Y.X.; Lan, Y.H. Backstepping Control of Speed Sensorless Permanent Magnet Synchronous Motor Based on Slide Model Observer. Int. J. Autom. Comput. 2015, 12, 149–155.
[55] Choi, C.; Lee, K.; Lee, W. Observer-Based Phase-Shift Fault Detection Using Adaptive Threshold for Rotor Position Sensor of Permanent-Magnet Synchronous Machine Drives in Electromechanical Brake. IEEE Trans. Ind. Electron. 2015, 62, 1964–1974.
[56] Foo, G.H.B.; Zhang, X.; Vilathgamuwa, D.M. A Sensor Fault Detection and Isolation Method in Interior Permanent-Magnet Synchronous Motor Drives Based on an Extended Kalman Filter. IEEE Trans. Ind. Electron. 2013, 60, 3485–3495.
[57] Sardar, M.U. Analysis of Broken Rotor Bar Diagnostic Techniques for Inverter Fed Induction Motor Faults. In Proceedings of the 22nd International Symposium “Topical Problems in the Field of Electrical and Power Engineering” and “Doctoral School of Energy and Geotechnology III”, Pärnu, Estonia, 23–26 August 2023.
[58] Asad, B.; Vaimann, T.; Kallaste, A.; Belahcen, A. Harmonic Spectrum Analysis of Induction Motor with Broken Rotor Bar Fault. In Proceedings of the 2018 IEEE 59th Annual International Scientific Conference on Power and Electrical Engineering, RTUCON, Riga, Latvia, 12–13 November 2018.
[59] Kumar, S.; Mukherjee, D.; Guchhait, P.K.; Banerjee, R.; Srivastava, A.K.; Vishwakarma, D.N.; Saket, R.K. A Comprehensive Review of Condition Based Prognostic Maintenance (CBPM) for Induction Motor. IEEE Access 2019, 7, 90690–90704.
[60] Dorrell, D.G.; Makhoba, K. Detection of Inter-Turn Stator Faults in Induction Motors Using Short-Term Averaging of Forward and Backward Rotating Stator Current Phasors for Fast Prognostics. IEEE Trans. Magn. 2017, 53, 1700107.
[61] Devi, N.R.; Siva Sarma, D.V.S.S.; Ramana Rao, P.V. Detection of Stator Incipient Faults and Identification of Faulty Phase in Three-Phase Induction Motor—Simulation and Experimental Verification. IET Electr. Power Appl. 2015, 9, 540–548.
[62] Tallam, R.M.; Lee, S.B.; Stone, G.C.; Kliman, G.B.; Yoo, J.; Habetler, T.G.; Harley, R.G. A Survey of Methods for Detection of Stator-Related Faults in Induction Machines. IEEE Trans. Ind. Appl. 2007, 43, 920–933.
[63] Jung, J.; Park, Y.; Lee, S.B.; Cho, C.; Kim, K.; Wiedenbrug, E.; Teska, M. Monitoring of Journal Bearing Faults Based on Motor Current Signature Analysis for Induction Motors. In Proceedings of the 2015 IEEE Energy Conversion Congress and Exposition, ECCE, Montreal, QC, Canada, 20–24 September 2015.
[64] Mirzaeva, G.; Saad, K.I. Advanced Diagnosis of Stator Turn-to-Turn Faults and Static Eccentricity in Induction Motors Based on Internal Flux Measurement. IEEE Trans. Ind. Appl. 2018, 54, 3961–3970.
[65] Halder, S.; Bhat, S.; Dora, B.K. Inverse thresholding to spectrogram for the detection of broken rotor bar in induction motor. Measurement 2022, 198, 111400.
[66] Kudelina, K.; Vaimann, T.; Rassolkin, A.; Kallaste, A.; Asad, B.; Demidova, G. Induction Motor Bearing Currents-Causes and Damages. In Proceedings of the 2021 28th InternationalWorkshop on Electric Drives: Improving Reliability of Electric Drives, IWED, Moscow, Russia, 27–29 January 2021.

[67] Shirazian, S.; Alibabaei, M. Using Neural Networks Coupled with Particle Swarm Optimization Technique for Mathematical Modeling of Air Gap Membrane Distillation (AGMD) Systems for Desalination Process. Neural Comput. Appl. 2017, 28, 2099–2104.

[68] Halder, S.; Bhat, S.; Zychma, D.; Sowa, P. Broken Rotor Bar Fault Diagnosis Techniques Based on Motor Current Signature Analysis for Induction Motor—A Review. Energies 2022, 15, 8569.

[69] Duque-Perez, O.; Garcia-Escudero, L.A.; Morinigo-Sotelo, D.; Gardel, P.E.; Perez-Alonso, M. Analysis of Fault Signatures for the Diagnosis of Induction Motors Fed by Voltage Source Inverters Using ANOVA and Additive Models. Electr. Power Syst. Res. 2015, 121, 1–13.

[70] Vilhekar, T.G.; Ballal, M.S.; Suryawanshi, H.M. Application of Multiple Parks Vector Approach for Detection of Multiple Faults in Induction Motors. J. Power Electron. 2017, 17, 972–982.

[71] Maouche, Y.; Oumaamar, M.E.K.; Boucherma, M.; Khezzar, A. Instantaneous Power Spectrum Analysis for Broken Bar Fault Detection in Inverter-Fed Six-Phase Squirrel Cage Induction Motor. Int. J. Electr. Power Energy Syst. 2014, 62, 110–117.

[72] Gangsar, P.; Tiwari, R. Signal Based Condition Monitoring Techniques for Fault Detection and Diagnosis of Induction Motors: A State-of-the-Art Review. Mech. Syst. Signal Process 2020, 144, 106908

[73] Zhang, P.; Du, Y.; Habetler, T.G.; Lu, B. A Survey of Condition Monitoring and Protection Methods for Medium-Voltage Induction Motors. IEEE Trans. Ind. Appl. 2011, 47, 34–46.

[74] Lin, C.K.; Liu, T.H.; Yu, J.T.; Fu, L.C.; Hsiao, C.F. Model-Free Predictive Current Control for Interior Permanent-Magnet Synchronous Motor Drives Based on Current Difference Detection Technique. IEEE Trans. Ind. Electron. 2014, 61, 667–681.

[75] Nguyen, V.; Seshadrinath, J.;Wang, D.; Nadarajan, S.; Vaiyapuri, V. Model-Based Diagnosis and RUL Estimation of Induction Machines under Interturn Fault. IEEE Trans. Ind. Appl. 2017, 53, 2690–2701.

[76] Yaghobi, H.; Arkan, M.; Perovi´c, D.K.; Unsworth, P.; Citation, O.; Chattopadhyay, S.; Mitra, M.; Sengupta, S.; Bengal, W.; Roshanfekr, R.; et al. Motor Current Signature Analysis to Detect Faults in Induction Motor Drives-Fundamentals, Data Interpretation, and Industrial Case Histories. IEEE Trans. Ind. Electron. 2017, 13.

[77] Kudelina, K.; Asad, B.; Vaimann, T.; Rassolkin, A.; Kallaste, A. Production Quality Related Propagating Faults of Induction Machines. In Proceedings of the 2020 11th International Conference on Electrical Power Drive Systems, ICEPDS, Saint Petersburg, Russia, 4–7 October 2020.

[78] Willwerth, A.; Roman, M. Electrical Bearing Damage—A Lurking Problem in Inverter-Driven Traction Motors. In Proceedings of the 2013 IEEE Transportation Electrification Conference and Expo: Components, Systems, and Power Electronics—From Technology to Business and Public Policy, ITEC, Metro Detroit, MI, USA, 16–19 June 2013.

[79] Kudelina, K.; Vaimann, T.; Asad, B.; Rassõlkin, A.; Kallaste, A.; Demidova, G. Trends and Challenges in Intelligent Condition Monitoring of Electrical Machines Using Machine Learning. Appl. Sci. 2021, 11, 2761.

[80] Dong, Z. A Study of Non-Stationary Signal Processing for Machinery Condition Monitoring. Ph.D. Thesis, School of Computing and Engineering, University of Huddersfield, Huddersfield, UK, 2012.

[81] Leite, V.C.M.N.; Borges Da Silva, J.G.; Veloso, G.F.C.; Borges Da Silva, L.E.; Lambert-Torres, G.; Bonaldi, E.L.; De Lacerda De Oliveira, L.E. Detection of Localized Bearing Faults in Induction Machines by Spectral Kurtosis and Envelope Analysis of Stator Current. IEEE Trans. Ind. Electron. 2015, 62, 1855–1865.

[82] Othman, M.S.; Nuawi, M.Z.; Mohamed, R. Vibration and Acoustic Emission Signal Monitoring for Detection of Induction Motor Bearing Fault. Int. J. Eng. Res. Technol. 2015, 4, 924–929.
[83] Wang, P.P.; Yu, Q.; Hu, Y.J.; Miao, C.X. Online Detection of Broken Rotor Bar Fault in Induction Motors by Combining Estimation of Signal Parameters via Min-Norm Algorithm and Least Square Method. Chin. J. Mech. Eng. (Engl. Ed.) 2017, 30, 1285–1295.
[84] Sapena-Bano, A.; Burriel-Valencia, J.; Pineda-Sanchez, M.; Puche-Panadero, R.; Riera-Guasp, M. The Harmonic Order Tracking Analysis Method for the Fault Diagnosis in Induction Motors under Time-Varying Conditions. IEEE Trans. Energy Convers. 2017, 32, 244–256.
[85] Sabir, H.; Ouassaid, M.; Ngote, N.; Benbouzid, M. A Novel Experimental Method to Detect Early Rotor Faults in InductionMachines. Int. J. Energy Convers. 2021, 9, 191.
[86] Ngote, N.; Guedira, S.; Ouassaid, M.; Cherkaoui, M.; Maaroufi, M. On the Monitoring of Rotor Fault in Induction Machine by the Use of the TSA Method Applied to Stator Current. Int. Rev. Electr. Eng. 2012, 7, 4822–4828.
[87] Ngote, N.; Ouassaid, M.; Guedira, S.; Cherkaoui, M. On the Detection of Induction-Motor Rotor Fault by the Combined "Time Synchronous Averaging-Discrete Wavelet Transform" Approach. J. Electr. Eng. Technol. 2015, 10, 2315–2325.
[88] Dey, S.; Roy, S.S.; Samanta, K.; Modak, S.; Chatterjee, S. Autocorrelation Based Feature Extraction for Bearing Fault Detection in Induction Motors. In Proceedings of the Proceedings—2019 International Conference on Electrical, Electronics and Computer Engineering, UPCON, Aligarh, India, 8–10 November 2019.
[89] Lu, S.; He, Q.; Yuan, T.; Kong, F. Online Fault Diagnosis of Motor Bearing via Stochastic-Resonance-Based Adaptive Filter in an Embedded System. IEEE Trans. Syst. Man. Cybern. Syst. 2017, 47, 1111–1122
[90] Braham, A.; Lachiri, Z. Diagnosis of Broken Bar Fault in Induction Machines Using Advanced Digital Signal Processing. Int. Rev. Electr. Eng. 2010, 5, 1460–1468.
[91] Dehina, W.; Boumehraz, M.; Kratz, F. Detectability of Rotor Failure for Induction Motors through Stator Current Based on Advanced Signal Processing Approaches. Int. J. Dyn. Control 2021, 9, 1381–1395.
[92] Granda, D.; Aguilar, W.G.; Arcos-Aviles, D.; Sotomayor, D. Broken Bar Diagnosis for Squirrel Cage Induction Motors Using Frequency Analysis Based on MCSA and Continuous Wavelet Transform. Math. Comput. Appl. 2017, 22, 30.
[93] Climente-Alarcon, V.; Antonino-Daviu, J.A.; Riera-Guasp, M.; Vlcek, M. Induction Motor Diagnosis by Advanced Notch FIR Filters and the Wigner-Ville Distribution. IEEE Trans. Ind. Electron. 2014, 61, 4217–4227.
[94] Kia, S.H.; Henao, H.; Capolino, G.A. A High-Resolution Frequency Estimation Method for Three-Phase Induction Machine Fault Detection. IEEE Trans. Ind. Electron. 2007, 54, 2305–2314.
[95] Martin-Diaz, I.; Morinigo-Sotelo, D.; Duque-Perez, O.; Arredondo-Delgado, P.A.; Camarena-Martinez, D.; Romero-Troncoso, R.J. Analysis of Various Inverters Feeding Induction Motors with Incipient Rotor Fault Using High-Resolution Spectral Analysis. Electr. Power Syst. Res. 2017, 152, 18–26.
[96] Lu, J.;Wang, P.; Duan, S.; Shi, L.; Han, L. Detection of Broken Rotor Bars Fault in Induction Motors by Using an Improved MUSIC and Least-Squares Amplitude Estimation. Math. Probl. Eng. 2018, 2018, 5942890.
[97] Alshorman, O.; Irfan, M.; Saad, N.; Zhen, D.; Haider, N.; Glowacz, A.; Alshorman, A. A Review of Artificial Intelligence Methods for Condition Monitoring and Fault Diagnosis of Rolling Element Bearings for Induction Motor. Shock. Vib. 2020, 2020, 8843759.

[98] Soualhi, A.; Clerc, G.; Razik, H. Detection and Diagnosis of Faults in Induction Motor Using an Improved Artificial Ant Clustering Technique. IEEE Trans. Ind. Electron. 2013, 60, 4053–4062.
[99] Nandi, S.; Ilamparithi, T.; Lee, S.B.; Hyun, D. Pole Pair and Rotor Slot Number Independent Frequency Domain Based Detection of Eccentricity Faults in Induction Machines Using a Semi On-Line Technique. In Proceedings of the 2009 IEEE International Symposium on Diagnostics for Electric Machines, Power Electronics and Drives, SDEMPED, Cargese, France, 31 August–3 September 2009.
[100] Di, C.; Bao, X.; Wang, H.; Lv, Q.; He, Y. Modeling and Analysis of Unbalanced Magnetic Pull in Cage Induction Motors with Curved Dynamic Eccentricity. IEEE Trans. Magn. 2015, 51, 8106507. [CrossRef]
[101] Saucedo-Dorantes, J.J.; Delgado-Prieto, M.; Osornio-Rios, R.A.; De Jesus Romero-Troncoso, R. Multifault Diagnosis Method Applied to an Electric Machine Based on High-Dimensional Feature Reduction. IEEE Trans. Ind. Appl. 2017, 53, 3086–3097.
[102] Toma, R.N.; Piltan, F.; Kim, J.M. A Deep Autoencoder-Based Convolution Neural Network Framework for Bearing Fault Classification in Induction Motors. Sensors 2021, 21, 8453.
[103] Yeh, C.C.; Povinelli, R.J.; Mirafzal, B.; Demerdash, N.A.O. Diagnosis of StatorWinding Inter-Turn Shorts in Induction Motors Fed by PWM-Inverter Drive Systems Using a Time-Series Data Mining Technique. In Proceedings of the 2004 International Conference on Power System Technology, POWERCON, Singapore, 21–24 November 2004; Volume 1.
[104] Romero-Troncoso, R.J.; Saucedo-Gallaga, R.; Cabal-Yepez, E.; Garcia-Perez, A.; Osornio-Rios, R.A.; Alvarez-Salas, R.; Miranda-Vidales, H.; Huber, N. FPGA-Based Online Detection of Multiple Combined Faults in Induction Motors through Information Entropy and Fuzzy Inference. IEEE Trans. Ind. Electron. 2011, 58, 5263–5270.
[105] Akar, M.; Cankaya, I. Broken Rotor Bar Fault Detection in Inverter-Fed Squirrel Cage Induction Motors Using Stator Current Analysis and Fuzzy Logic. Turk. J. Electr. Eng. Comput. Sci. 2012, 20, 1077–1089.
[106] Bozorgi, A.M.; Farasat, M.; Jafarishiadeh, S. Improved Model Predictive Current Control of Permanent Magnet Synchronous Machines with Fuzzy Based Duty Cycle Control. In Proceedings of the ECCE 2016—IEEE Energy Conversion Congress and Exposition, Milwaukee, WI, USA, 18–22 September 2016.
[107] Tao, H.; Peng, T.; Yang, C.; Gao, J.; Yang, C.; Gui, W. Voltage and Current Sensor Fault Diagnosis Method for Traction Converter with Two Stator Current Sensors. Sensors 2022, 22, 2355.
[108] Kraleti, R.S.; Zawodniok, M.; Jagannathan, S. Model Based Diagnostics and Prognostics of Three-Phase Induction Motor for Vapor Compressor Applications. In Proceedings of the PHM 2012—2012 IEEE International Conference on Prognostics and Health Management: Enhancing Safety, Efficiency, Availability, and Effectiveness of Systems through PHM Technology and Application, Conference Program, Denver, CO, USA, 18–21 June 2012.
[109] Jigyasu, R.; Shrivastava, V.; Singh, S. Smart Classifier Based Prognostics and Health Management of Induction Motor. Mater. Today Proc. 2020, 43, 355–361
[110] Lombard, Patrick, Fireteanu, Virgiliu, and Constantin, Alexandru-Ionel. ‘Influences on the Electromagnetic Torque and Rotor Force of Different Faults in Squirrel-cage Induction Motors’. 1 Jan. 2019 : 805 – 815. DOI: 10.3233/JAE-171136
[111] A. -I. CONSTANTIN, "Detection Based on Stator Current Signature of the Single and Combined Short-Circuit, Broken Bar and Eccentricity Faults in Induction Motors," 2019 11th International Symposium on Advanced Topics in Electrical Engineering (ATEE), Bucharest, Romania, 2019, pp. 1-6, doi: 10.1109/ATEE.2019.8724984.
[112] Altair Flux 3D documentation